



NJC

Probing magnetic and vibrational properties of trigonal-bipyramidal Co(II) and Ni(II) complexes using advanced spectroscopic techniques

Journal:	<i>New Journal of Chemistry</i>
Manuscript ID	NJ-ART-01-2025-000184.R1
Article Type:	Paper
Date Submitted by the Author:	25-Feb-2025
Complete List of Authors:	Jenkins, Michael; University of Tennessee, Department of Chemistry Ozerov, Mykhaylo; Florida State University, National High Magnetic Field Laboratory Krzystek, Jurek; National High Magnetic Field Laboratory, Condensed Matter Science Daemen, Luke; Oak Ridge National Laboratory Cheng, Yongqiang; Oak Ridge National Laboratory Xue, Zi-Ling; University of Tennessee, Department of Chemistry

SCHOLARONE™
Manuscripts

Probing magnetic and vibrational properties of trigonal-bipyramidal Co(II) and Ni(II) complexes using advanced spectroscopic techniques

Michael J. Jenkins,^a Mykhaylo Ozerov,^b J. Krzystek,^b Luke L. Daemen,^c Yongqiang Cheng,^c Zi-Ling Xue^{*,a}

^a *Department of Chemistry, University of Tennessee, Knoxville, Tennessee 37996, USA*

^b *National High Magnetic Field Laboratory, Florida State University, Tallahassee, Florida 32310, USA*

^c *Neutron Scattering Division, Oak Ridge National Laboratory, Oak Ridge, Tennessee 37831, USA*

Abstract

Transition metal-based single-molecule magnets (SMMs) with local C_3 or higher symmetries on the metal centers have garnered significant interest due to their unique magnetic properties. With rhombic anisotropy parameters $E =$ (or \approx) 0 for such highly symmetric complexes, quantum tunneling in magnetic relaxation is eliminated or reduced, enhancing the performance of the SMMs. Zero-field splitting (ZFS) in metal complexes has been probed by various advanced methods, including spectroscopies such as far-infrared magneto-spectroscopy (FIRMS), high-frequency and -field electron paramagnetic resonance (HFEP), and inelastic neutron scattering (INS). Studies of the trigonal bipyramidal SMM complex with local C_{3v} symmetry, $(Me_4N)[Co(MST)(OH_2)]$ (**Co-MST-H₂O**, $MST^{3-} = N,N',N''$ -[2,2',2''-nitriлотris(ethane-2,1-diyl)]tris(2,4,6-trimethylbenzenesulfonamido)), give the following spin-Hamiltonian parameters: axial ($D = 25.3 \text{ cm}^{-1}$) and rhombic ($E = 0$) ZFS values, $g_{\perp} = 2.23$, and $g_{\parallel} = 2.045$. Phonon properties of **Co-MST-H₂O** have been studied by INS and DFT phonon calculations, yielding phonon symmetries, energies, and movies. Phonons here refer to either molecular vibrations (internal modes) or lattice vibrations (external modes or intermolecular vibrations) in the crystalline solid. Intermolecular interactions in **Co-MST-H₂O** have been probed by Hirshfeld surface analysis, revealing strong interactions between the $[Co(MST)(OH_2)]^{-}$ anion and solvents (H_2O and CH_2Cl_2) in the crystal lattice. The DFT phonon calculations of **Co-MST-H₂O** have also generated the spin density on the Co^{2+} ion and other atoms in the molecule. For $(Me_4N)[Ni(MST)(OH_2)]$ (**Ni-MST-H₂O**), FIRMS and INS studies did not show the magnetic transitions among the spin sublevels. Spin-Hamiltonian parameters (D , E , and g value) of **Ni-MST-H₂O**, determined by magnetometry, were reported earlier (K.A. Schulte, K.R. Vignesh, K.R. Dunbar, *Chem. Sci.*, 2018, **9**, 9018). In the absence of magnetic resonance or INS results

for the magnetic transitions in **Ni-MST-H₂O**, magnetometry is the viable technique to determine spin-Hamiltonian parameters for the compound. Hirshfeld surface analysis of **Ni-MST-H₂O** shows strong interactions of the [Ni(MST)(OH₂)]⁻ anion with lattice solvent H₂O and the cation Me₄N⁺.

Introduction

Magnetic properties of transition metal complexes have been of intense recent interest for their potential uses as quantum materials with applications in spintronics, data storage, and quantum computing.¹⁻²⁰ d-Block complexes with at least two unpaired electrons ($S \geq 1$) and quenched first-order spin-orbit coupling (SOC), showing a barrier (U) to spin reversal (or magnetic relaxation) are considered single-molecule magnets (SMMs).^{13, 21} One research area is to find SMMs with large and tunable U . Magnetic anisotropy of transition metal complexes is far more tunable than lanthanide complexes, as the ligand field effects are more easily tuned in the former than the spin-orbit coupling (SOC) in the latter.^{3, 4, 16, 17, 22-24} Transition metal complexes with many unpaired electrons (and thus large spins) are favored, as the increase in the spin (S) leads to the increase in the energy barrier (U) for spin reversal. Because of ligand field or Jahn-Teller distortion, many transition metal complexes have quenched angular orbital momentum of the unpaired electrons. The magnetic properties of such complexes are governed by the second-order SOC, as represented by zero-field splitting (ZFS).²⁵⁻³⁶ The magnitude of the ZFS for a transition metal complex is given by axial (D) and rhombic (E) anisotropy parameters, as defined by spin Hamiltonian in Eq. 1:

$$\hat{H}_S = D[\hat{S}_z^2 - \frac{S(S+1)}{3}] + E(\hat{S}_x^2 - \hat{S}_y^2) + \mu_B g_x B_x \hat{S}_x + \mu_B g_y B_y \hat{S}_y + \mu_B g_z B_z \hat{S}_z \quad (1)$$

where \hat{S} is the spin operator, μ_B is the electron Bohr magneton, $g_{x,y,z}$ are the g -factor components, and $B = (B_x, B_y, B_z)$ is the applied magnetic field vector.³⁷⁻³⁹ In Eq. 1, the last three terms show the Zeeman effect on the zero-field split states.

For complexes with at least C_3 crystallographic point group symmetry at the metal site (or the paramagnetic center), spin Hamiltonian is given in Eq. 2:

$$\hat{H}_S = D[\hat{S}_z^2 - \frac{S(S+1)}{3}] + \mu_B g_{||} B_z \hat{S}_z + \mu_B g_{\perp} (B_x \hat{S}_x + B_y \hat{S}_y) \quad (2)$$

where g_{\parallel} and g_{\perp} are the g -tensor components parallel and perpendicular, respectively, to the unique z axis.

Using the ZFS parameters, the energy barrier (U) for a compound is given by Eqs. 3-4:

$$U = |D|(S^2 - \frac{1}{4}) \text{ for non-integer spins} \quad (3)$$

$$U = |D|(S^2) \text{ for integer spins} \quad (4)$$

Penta-coordinate Co^{2+} complexes have been actively studied to use their magnetic anisotropies in the search of SMMs.^{22, 24, 26, 35, 37, 40-56} For complexes with at least C_3 crystallographic point group symmetry of the metal site (or the paramagnetic center), the rhombic ZFS parameter $E = 0$.^{24, 37, 55, 56} Five-coordinate Co^{2+} -based SMMs with such crystallographic symmetries are typically trigonal bipyramidal in the C_{3v} ^{49, 53, 54} or D_{3h} ³³ point group. These symmetries give d orbital configuration in Figure 1a with quenched first-order SOC. Thus, mixing of the $M_S = \pm 1/2$ and $M_S = \pm 3/2$ states (to give ϕ_1, ϕ_2, ϕ_3 , and ϕ_4 , as shown in Figure 1b which leads to quantum tunneling) does *not* occur. Five-coordinate Co^{2+} -based SMMs with crystallographic C_{3v} or D_{3h} symmetry through the metal ion are therefore highly desirable. However, there are few five-coordinate Co^{2+} SMMs with such high symmetries.^{33, 49, 53, 54} Instead, some five-coordinate Co^{2+} SMMs have *approximate* (or *local*) C_3 ^{22, 34, 45, 53, 57-59} or C_4 ^{26, 60} symmetries of the metal sites. Either crystallographic space groups^{26, 34, 45, 53, 57-59} in, e.g., monoclinic unit cells (with C_2 or C_{2h} symmetry), or the ligands^{22, 60} such as N_3^- or NCS^- with bent structures, lower the symmetries of the complexes. In addition, five-coordinate Co^{2+} SMMs with planar, tri-dentate ligands such as $\text{Co}(\text{terpy})\text{X}_2$ (terpy = terpyridine)^{61, 62} or analogs^{52, 63-68} have approximately C_{2v} symmetry around the metal ions. For such complexes in which the crystallographic point group symmetry of the metal site is lower than C_3 , $E \neq 0$ and $2D' = 2(D^2 + 3E^2)^{1/2}$, giving the ground-state quartet level in Figure 1b, in which mixing of the $M_S = \pm 1/2$ and $M_S = \pm 3/2$ states (to give ϕ_1, ϕ_2, ϕ_3 , and ϕ_4) occurs, potentially leading to quantum tunneling and fast magnetic relaxation. These are undesirable properties for SMMs.

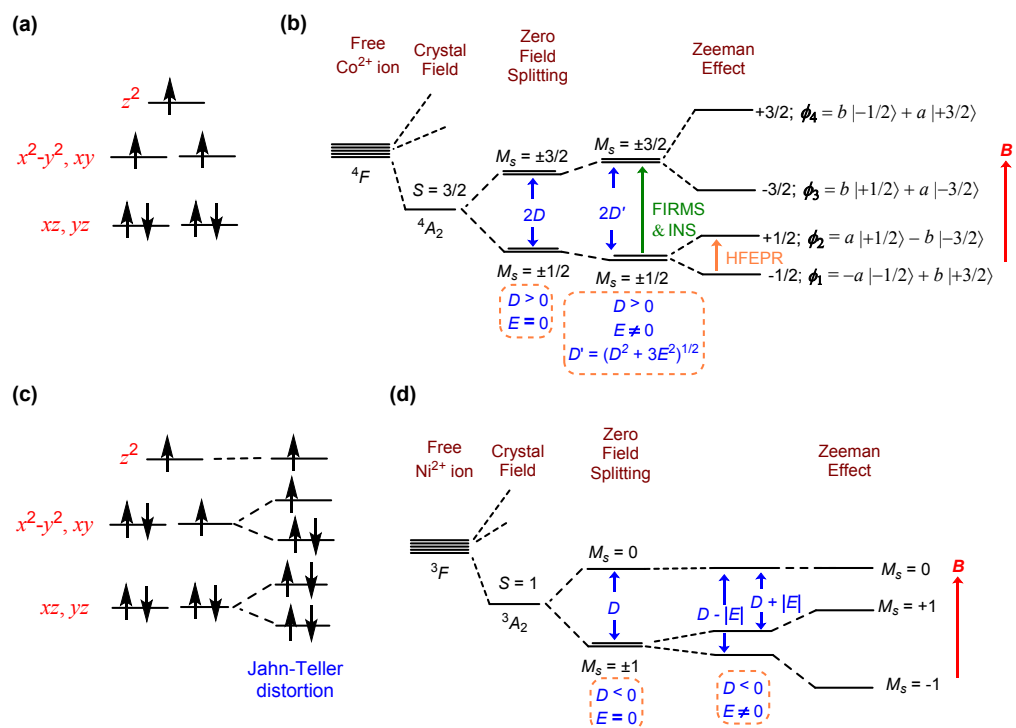


Figure 1. (a) Ligand field splitting diagram for a 5-coordinate, high-spin Co^{2+} complex in crystallographic C_{3v} or D_{3h} symmetry through the metal ion. (b) Ground-state quartet spin levels in high-spin, d^7 complexes with at least C_3 crystallographic point group symmetry of the metal site ($D > 0$; $E = 0$) and lower symmetry ($D > 0$; $E \neq 0$). When the symmetry is lower than C_3 , $E \neq 0$ and there is a mixing of states to give ϕ_1 , ϕ_2 , ϕ_3 , and ϕ_4 . The mixing coefficients $a = \cos \beta$ and $b = \sin \beta$ are described by the mixing angle β obtained from the spin-Hamiltonian ($S = 3/2$).^{39, 69} Mixing depends on the rhombicity as $\tan 2\beta = \sqrt{3} (E/D)$. (c) Ligand field splitting diagram for a high-spin Ni^{2+} complex in C_{3v} geometry with the Jahn-Teller distortion.^{20, 70} (d) Ground-state quartet spin levels in high-spin, d^8 complexes with at least at least C_3 crystallographic point group symmetry of the metal site ($D < 0$; $E = 0$ before the Jahn-Teller distortion) and lower symmetry ($D < 0$; $E \neq 0$) after the Jahn-Teller distortion.

Penta-coordinate d^8 Ni^{2+} complex with crystallographic C_{3v} symmetry through the metal ion has been reported.^{20, 70} However, Jahn-Teller distortion leads to the splitting of degenerate d orbitals (Figure 1c). There are also penta-coordinate Ni^{2+} complexes with *approximate* (or *local*) C_{3v} ^{35, 57, 71-75} or C_{4v} ^{76, 77} symmetries. Their crystal structures or ligands lower the symmetries of the complexes.

A series of transition metal complexes containing the tripodal ligand N,N',N'' -[2,2',2''-nitrilotris(ethane-2,1-diyl)]tris(2,4,6-trimethylbenzenesulfonamido) (MST^{3-} , Figure 2) were

1
2
3 reported by Lacy, Lau, Borovik and coworkers, revealing catalytic activities.^{74, 78, 79}

4 Later, magnetic properties of $[\text{NMe}_4][\text{Co}(\text{MST})(\text{OH}_2)]$ (**Co-MST-H₂O**) and $[\text{NMe}_4][\text{Ni}(\text{MST})(\text{OH}_2)]$
5 (**Ni-MST-H₂O**) were reported by Schulte, Vignesh, and Dunbar, showing slow magnetic
6 relaxation and SMM properties.⁵⁷ Although the local symmetry for both $[\text{NMe}_4][\text{Co}(\text{MST})(\text{OH}_2)]$
7 (**Co-MST-H₂O**) and $[\text{NMe}_4][\text{Ni}(\text{MST})(\text{OH}_2)]$ (**Ni-MST-H₂O**) is C_{3v} , the crystallographic symmetry
8 of the two complexes at 100 K is triclinic $P\bar{1}$ (No. 2; point group C_1).⁵⁷ ZFS parameters were
9 determined from reduced magnetization data, giving spin-Hamiltonian parameters for **Co-MST-**
10 **H₂O** ($D = 24 \text{ cm}^{-1}$, $|E| = 0.001 \text{ cm}^{-1}$, $g = 2.40$) and **Ni-MST-H₂O** ($D = -209 \text{ cm}^{-1}$, $|E| = 1.8 \text{ cm}^{-1}$,
11 $g = 2.81$).
12
13

14
15
16
17 Magnetometry is an indirect, non-resonant method for determining ZFS parameters.
18 There are several reported spectroscopic techniques for directly determining ZFS,^{80, 81} including
19 high-frequency and -field electron paramagnetic resonance (HFEP),^{26, 29, 31, 36, 46, 54, 65, 67, 82-87}
20 far-IR magneto-spectroscopy (FIRMS),^{29, 47, 70, 88-100} and inelastic neutron scattering (INS).¹⁰¹⁻¹¹⁷
21 HFEP is a powerful tool to measure ZFS up to approximately 32 cm^{-1} for non-Kramers ions,
22 and 15 cm^{-1} for Kramers spin species using, e.g., the facilities at the US National High Magnetic
23 Field Laboratory (NHMFL).^{80, 82, 91, 118} For ZFS $>32 \text{ cm}^{-1}$, a combined use of HFEP and
24 FIRMS⁸¹ has been adopted to determine large spin-Hamiltonian parameters.^{29, 46, 65, 67, 84, 92, 93, 95-}
25 ⁹⁸ FIRMS is far-IR spectroscopy conducted with variable magnetic fields, helping reveal
26 magnetic transitions in the spectra.⁸¹ Phonon properties of metal complexes and intermolecular
27 interactions are important to the understanding of spin-phonon coupling and magnetic
28 relaxation. Indirect-geometry time-of-flight (TOF) INS spectroscopy has been widely used to
29 probe both magnetic and vibrational transitions.¹⁰³ Incident neutrons (with spin $\frac{1}{2}$) interact with
30 both unpaired electrons and nuclei of atoms in the sample, leading to magnetic and vibrational
31 transitions, respectively.¹⁰³ Unlike HFEP and FIRMS that use external magnetic fields to probe
32 magnetic transitions, indirect-geometry INS spectroscopy can distinguish magnetic transitions in
33 spectra from vibrational transitions (also known as phonons) *without* the use of external
34 magnetic fields. Phonons here refer to either molecular vibrations (internal modes) or lattice
35 vibrations (external modes or intermolecular vibrations) in crystalline solids of compounds.
36 Phonons are bosons following Bose-Einstein statistics, while electrons, giving magnetic
37 transitions, are fermions following Boltzmann statistics. Thus, in variable-temperature (VT) INS
38 spectra, magnetic and phonon peaks show different temperature profiles, leading to their
39 identifications. Another unique feature of INS is that it does not have symmetry-based selection
40 rules for phonons/vibrations, unlike optical IR and Raman spectroscopies each with its own
41 selection rules.¹⁰³ Thus, *all* phonons are observed in INS spectra. In addition, powerful DFT
42
43
44
45
46
47
48
49
50
51
52
53
54
55
56
57
58
59
60

phonon calculations give calculated phonon symmetries, energies, and INS *phonon* spectra. Thus, INS and the calculations together are very useful to probe magnetic and phonon properties of metal complexes.¹⁰³ Direct determination of ZFS and spin-Hamiltonian parameters by the advanced spectroscopies has led to their increased use.^{25, 82, 84, 101, 104, 119-124} The DFT phonon calculations also give spin densities on atoms in the molecules.

Hirschfeld surface analysis is a unique technique to probe intermolecular interactions in the context of crystal packing.^{121, 125} It has been extensively used to probe such interactions in metal complexes, including SMMs and other magnetic compounds.^{68, 126-148} Thus, Hirschfeld surface analysis and phonon studies, which include lattice vibrations (external modes), provide an understanding of intermolecular interactions from two perspectives.

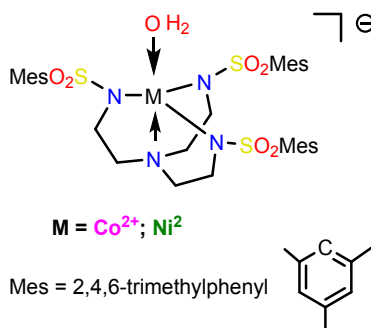


Figure 2. Structures of the anions in **Co-MST-H₂O** and **Ni-MST-H₂O**. Both show local C_{3v} symmetry.

We have studied **Co-MST-H₂O** and **Ni-MST-H₂O** to answer the following: (1) Could the ZFS and other spin-Hamiltonian parameters be determined using advanced spectroscopies? How are the results compared with those from DC magnetic susceptibility and reduced magnetization? (2) What are the phonon properties of the two complexes, including their symmetries, as revealed by inelastic neutron scattering (INS) spectroscopy and DFT phonon calculations? (3) How do molecules of the two complexes interact in their crystalline solids? Our studies are reported here.

Results and discussion

[NMe₄][Co(MST)(OH₂)] (**Co-MST-H₂O**)

Co-MST-H₂O has been probed by far-IR magneto-spectroscopy (FIRMS), HFEPR, INS, DFT-phonon calculations, and Hirschfeld surface analysis.

FIRMS

The FIRMS we have used has a typical energy range of 12–720 cm^{-1} . Since the energy gaps between the spin sublevels in SMMs are often in that energy range, far-IR (i.e., FIRMS) is selected to probe them. A transition from ground $M_S = \pm 1/2$ sublevel to the excited $M_S = \pm 3/2$ sublevel is magnetic dipole-allowed.^{81, 149, 150} IR-active phonons are also observed in far-IR. To identify the magnetic peaks from phonon peaks in far-IR spectra, variable magnetic fields are used. The former shift with the fields because of Zeeman effect (Figure 1), while the latter do not. The experimental set up in FIRMS is analogous to that of a typical IR experiment, except that the sample is placed inside a magnet and, in our studies, at 5 K. Powders of the sample were made to a mull in *n*-eicosane, a waxy substance transparent in the far-IR range.

Changes by the external magnetic fields in FIRMS spectra of **Co-MST-H₂O** at 0 and 17 T are observable in Figure 3a. To distinguish the magnetic transitions from the phonon peaks, all spectra were normalized to the reference spectrum, which is the average spectrum for all magnetic fields at 0-17 T. Figure 3b shows the normalized 2D plot (known as the heatmap or contour map). In the 2D plot, a magnetic peak is clearly observed at 50.6(6) cm^{-1} , which blue-shifts as a result of transitions from the Zeeman-split sublevels. The magnetic peak at zero field is the $M_S = \pm 1/2 \rightarrow M_S = \pm 3/2$ transition (Figure 1b). That is, ZFS for **Co-MST-H₂O**: $2D' = 2(D^2 + 3E^2)^{1/2} = 50.6(6) \text{ cm}^{-1}$. However, determining the *D* and *E* values requires additional results from HFEPFR discussed below. Also, no spin-phonon coupling is obvious, as no avoided crossing is clear in Figure 3b. In addition to the dominant zero-field transition at 50.6(6) cm^{-1} , another broad transition was observed at 65(1) cm^{-1} (Figure 3c-d). It has a very low signal/noise (*S/N*) ratio and we would be reluctant to claim it is a real resonance, but it coincides very well with the magnetometric result for *D* of the de-hydrated complex $[\text{NMe}_4][\text{Co}(\text{MST})]$ (**Co-MST**) ($2D' = 66 \text{ cm}^{-1}$)⁵⁷ and is corroborated by HFEPFR (see below). We thus tentatively identify it as originating from the dehydrated derivative **Co-MST**. Given the propensity of **Co-MST-H₂O** to lose the coordinated water molecule, it is conceivable that the sample of **Co-MST-H₂O** partially lost water during the sample cooling process which involves pumping on it, to give a small amount of **Co-MST**.

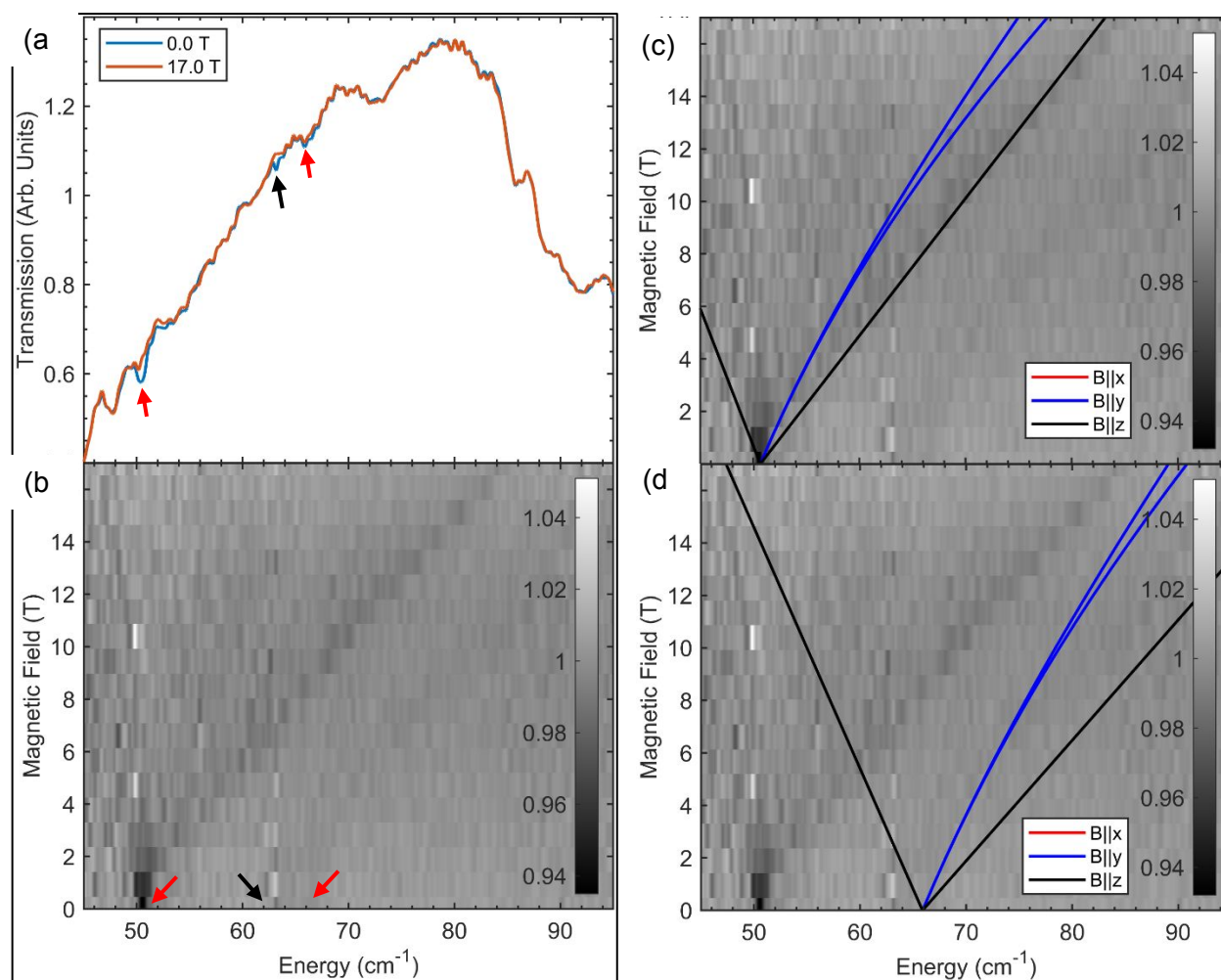


Figure 3. FIRMS of a powder sample of **Co-MST-H₂O**. (a) Spectra at 5 K and 0 and 17 T. (b) Contour plot of the normalized (by average) transmission, showing blue shifting of the magnetic peak at 50.6(6) cm^{-1} . The red arrows point to the magnetic transitions. The black arrow points to a shot noise in the spectra. There is no clear spin-phonon coupling or avoided crossings. (c) Turning points for the magnetic peak at 50.6(6) cm^{-1} as solid lines simulated by *EasySpin* in the powder spectra using g -values from HFEPR. (d) Turning points for the weak magnetic peak of **Co-MST** at 65(1) cm^{-1} as solid lines simulated by *EasySpin* in the powder spectra using g -values from HFEPR. Additional FIRMS results of **Co-MST-H₂O** are given in Figure S2 (ESI).

HFEPR

HFEPR is a field-domain version of magnetic resonance, and can deliver information complementary to FIRMS. When applied to compound **Co-MST-H₂O** in a loose polycrystalline form, at low temperatures, it delivers spectra such as shown in Figure S4 in ESI. The shape of

1
2
3 the spectra strongly suggests that the compound torques (aligns) with magnetic field, a
4 phenomenon well known to HFEPR spectroscopists.⁸³ The spectra are thus similar to those of a
5 single crystal. However, in such a case one would expect a single resonance corresponding to
6 the intra-Kramers transition between the $M_S = \pm 1/2$ sublevels while two resonances of unequal
7 intensities are actually observed. This observation suggests the presence of two different spin
8 species. The frequency dependence of the two resonances (Figure S5) shows that the two
9 species differ by their g -values. We can thus tentatively attribute the resonances to complexes
10 **Co-MST-H₂O** and its anhydrous derivative (Me₄N)[Co(MST)] (**Co-MST**) produced by the loss of
11 the axial water ligand. We tentatively attribute the lower-intensity resonance with higher g_{\perp} value
12 to the anhydrous species.

13
14 Given that the field-aligned spectra were uninformative with regard to spin-Hamiltonian
15 parameters, we proceeded to prevent the torquing by pressing **Co-MST-H₂O** in a pellet with *n*-
16 eicosane. The resulting spectra at 203 GHz are shown in Figure 4 and can be recognized as
17 originating from a powder rather than a single crystal. At low temperatures (10 K in Figure 4a),
18 the powder pattern corresponds to a single species, which is assigned to
19 [NMe₄][Co(MST)(OH₂)] (**Co-MST-H₂O**), as proved by the simulation that uses the $2D'$ -value
20 obtained from FIRMS, 50.6 cm⁻¹. The other spin-Hamiltonian parameters used in the simulation
21 are: $E = 0$, $g_{\perp} = 2.23$, $g_{\parallel} = 2.045$. The ZFS and g -tensors are thus strictly axial and the D' value
22 obtained from FIRMS is equal to D .

23
24 Raising the temperature (40 K in Figure 4b) causes an emergence of a second parallel
25 turning point in the spectrum at ca. 6.2 T, of lower intensity. The perpendicular turning point
26 remains unsplit at the same position (3.3 T). This corresponds to a second spin species whose
27 spin-Hamiltonian parameters were obtained through simulation: $E = 0$, $g_{\perp} = 2.23$, $g_{\parallel} = 2.33$.
28 Apparently, embedding the sample in an *n*-eicosane pellet did not fully prevent it from losing
29 water under vacuum. Alternatively, the pressure exerted on the sample while making the pellet
30 may have caused a release of coordinated water, creating the de-hydrated species **Co-MST**.
31 The simulation of that extra species used the tentative D -value of the second spin species, i.e.,
32 32.5 cm⁻¹ observed by FIRMS. This species thus has a much larger g_{\parallel} value than the first one
33 but the same g_{\perp} value. For both species, the rhombicity factor E/D remains zero within the
34 linewidth of the perpendicular turning point.

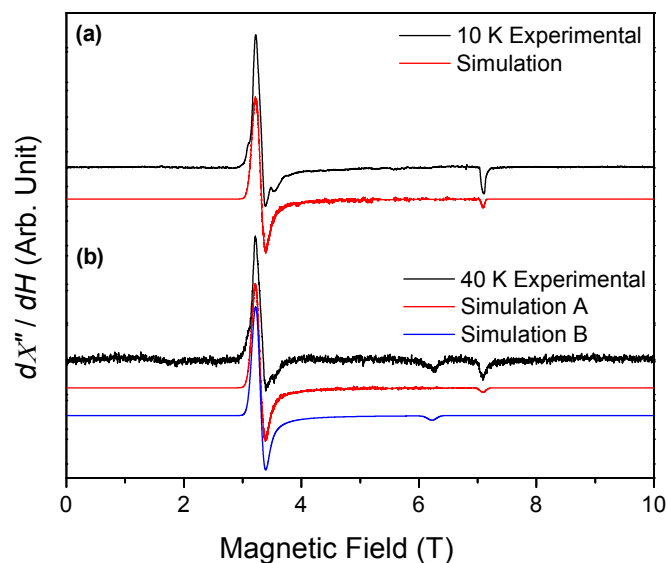


Figure 4. (Top) HFEPR spectrum of **Co-MST-H₂O** embedded in an *n*-eicosane pellet at 10 K and 203 GHz (black trace) accompanied by a powder simulation (red trace) using spin-Hamiltonian parameters: $D = 25.3 \text{ cm}^{-1}$, $E = 0$, $g_{\perp} = 2.23$, $g_{\parallel} = 2.045$. (Bottom) HFEPR spectrum of the same sample at 40 K (black trace) accompanied by simulations. For species A (red trace), the simulation parameters are the same as at 10 K; for species B (blue trace), the parameters are: $D = 32.5 \text{ cm}^{-1}$, $E = 0$, $g_{\perp} = 2.23$, $g_{\parallel} = 2.33$. dX''/dH is the first derivative of the absorption X'' vs the external magnetic field H .

INS

As discussed earlier, variable-temperature (VT) INS (without using external magnetic fields) is required to differentiate between vibrational/phonon and magnetic excitations. As phonons and electrons respond differently to temperature changes, the use of Bose-corrected VT-INS may determine which excitations are magnetic or phonon/vibrational.¹⁰³

INS of **Co-MST-H₂O** was conducted using Vibrational Spectrometer, known as VISION, at Oak Ridge National Laboratory (ORNL). There are forward- and back-scattering detectors at VISION, which are 45° and 135° from the incident neutrons, respectively.¹⁰³ The sample was sealed inside a sample can under a helium atmosphere in a glovebox and spectra were collected at 5, 25, 50, 75, 100, and 125 K. Bose-corrected VT INS are given in Figure 5, where Bose correction is a numerical normalization that highlights non-phonons by applying normalization to phonons that follow Bose-Einstein statistics. The peak at 48.5 cm^{-1} is assigned to the magnetic transition in **Co-MST-H₂O**, which is slightly shifted from 50.6 cm^{-1} observed in

FIRMS likely due to instrument errors. Spin-Hamiltonian parameters determined by the advanced techniques: $D = 25.3 \text{ cm}^{-1}$, $E = 0$, $g_{\perp} = 2.23$, and $g_{\parallel} = 2.045$, are very close to $D = 24 \text{ cm}^{-1}$, $|E| = 0.001 \text{ cm}^{-1}$, $g = 2.40$ determined using magnetometry by Schulte, Vignesh, and Dunbar.⁵⁷

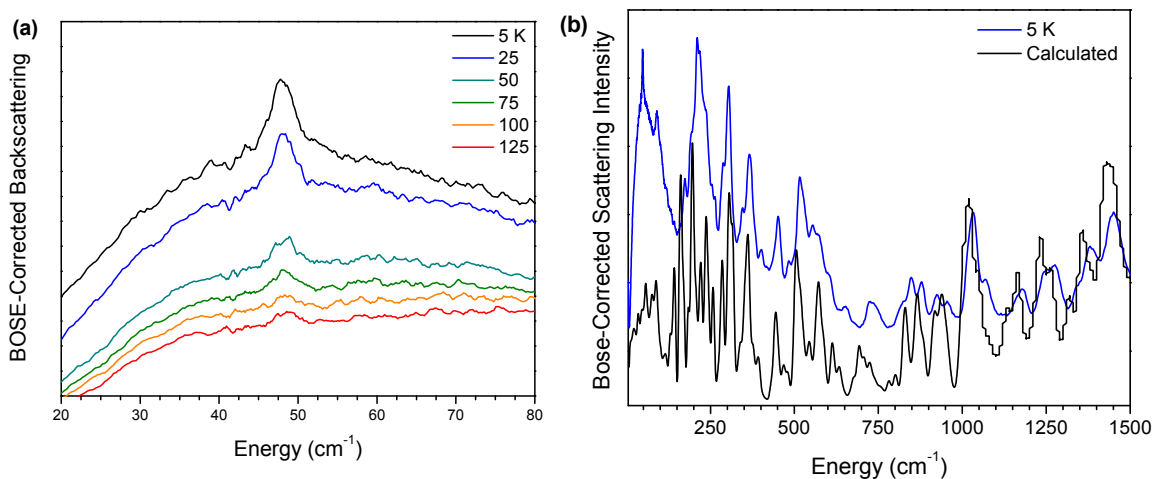


Figure 5. (a) Bose-corrected INS spectra of **Co-MST-H₂O** at 20-80 cm^{-1} . Forward-scattering spectra are given in Figure S6. (b) INS spectrum at 5 K in comparison to the calculated INS spectrum in the 5-1500 cm^{-1} range.

DFT phonon and spin density calculations

The phonon INS spectrum for **Co-MST-H₂O** was calculated using the periodic DFT VASP (Vienna Ab Initio Simulation) program. The calculated INS spectrum is compared with the experimental INS spectrum at 5 K. *Ab initio* (also known as first-principle) DFT calculations allow for predictions of interatomic force constants. For **Co-MST-H₂O**, the calculated spectrum overall matches experimental spectrum well.

Calculated symmetries and energies of phonons are given in Table S1 in ESI. There are four phonons (47.65, 50.62, 53.95, and 54.59 cm^{-1}) near the magnetic excitation at 48.5 cm^{-1} , as predicted by VASP calculations. Among the four phonons (listed in Table 1), only the 54.59 cm^{-1} phonon has the u symmetry which is far-IR active. However, there is no observable spin-phonon coupling with this phonon in FIRMS (Figure 3) as avoided crossing. Movies of these calculated phonons are given in electronic supplementary material (ESI).

Table 1. List of calculated phonons near the magnetic transition in **Co-MST-H₂O** and their symmetries from VASP calculations

Frequency (cm ⁻¹)	Symmetry
47.65	<i>A_g</i>
50.62	<i>A_g</i>
53.95	<i>A_g</i>
54.59	<i>A_u</i>

The DFT calculation of phonons produced phonon movies for the four phonons in Table 1, which are given in ESI. These phonon movies of the anion (**Co-MST-H₂O**⁻) in **Co-MST-H₂O** show small changes in the location of the Co²⁺ ion of the molecule. Larger changes in the mesityl positions in the MST³⁻ ligand and shifting of the water molecule are the more noticeable in the phonon movies.

The DFT phonon calculations also determined the spin density, ρ_s , on the Co²⁺ ion in **Co-MST-H₂O**, providing a quantitative scale, revealing how the spin is dispersed onto Co²⁺ ion and atoms in the ligand.¹⁵¹ VASP partitions electrons according to the Wigner-Seitz radius a_e in Eq. 5:¹⁵²

$$a_e = (3/4\pi n_e)^{1/3} \quad (5)$$

where n_e is the particle density of electrons; a_e is the radius “occupied” by one atom in a sample, and each atom is considered as a sphere.

The calculations do not include the spin densities residing in the bonds, but rather just the densities in individual atoms. The range of spin densities for each atom type is presented in Table 2. Detailed spin densities are given in Table S2. The total spin density (sum of those on all atoms) on the **Co-MST-H₂O** molecule is 2.863 which is lower than 3 (= 3 unpaired electrons). The total spin density here is similar those in, e.g., in Co(PPh₃)₂Cl₂ (2.797),⁸⁴ Co(PPh₃)₂Br₂ (2.783),⁸⁴ and Co(PPh₃)₂I₂ (2.747).⁸⁴ The remaining spin densities are dispersed in the *bonds* in the **Co-MST-H₂O** molecule. *No spin densities are present in the atoms of the cation NMe₄⁺ or lattice solvents (H₂O and CH₂Cl₂).* In other words, the unpaired electron spins appear to be entirely on the Co²⁺-containing anion [Co(MST)(OH₂)]⁻. We have used the current DFT calculation method to obtain spin densities in several Co²⁺ SMMs (Table 2).^{46, 84} It is the first

time that spin densities entirely on the metal-containing anion have been observed.

Most of the spin densities, 2.627 (87.6% of the 3 unpaired electrons) of the total 2.863, is concentrated on the Co^{2+} ion. This is understandable as the unpaired electrons are in the Co^{2+} ion. Then, the axial N atom (N3 in Table S2) bound to the Co^{2+} ion has the next highest spin density of 0.045, followed by the 3 equatorial N atoms (N1, N5, N7; spin densities: 0.036-0.037) and the O atom of the water ligand (O3; 0.030) that all bind directly to the Co^{2+} ion. After these α atoms (bound to Co^{2+}), β atoms have much smaller or no spin densities, including 0.004-0.005 for S atoms, -0.001 for the C atoms (C13, C23, C33) bound to the 3 equatorial N atoms, -0.001 to 0 for the C atoms (C5, C21, C31) bound to the axial N atom, and 0 for the 2 H atoms of the water ligand. The negative spin densities here indicate that these (small) spins are in the *opposite* direction as the 3 unpaired electrons on the molecule. Some of the other atoms of the ligand, including a few H atoms, carry small spin densities (Table S2). A comparison of calculated spin densities on Co^{2+} ions in a few complexes and their ZFS D' values are given in Table 2.

Table 2. Correlation between calculated spin densities on the Co^{2+} ions and ZFS parameters of the complexes/coordination polymer (CP)

Complexes	Spin densities on the Co^{2+} ions (and percentage of 3 unpaired electrons)	D' values (cm^{-1})	Refs
$\text{Co}(\text{PPh}_3)_2\text{I}_2$	2.553 (85.1%)	13.63(10)	84
$\text{Co}(\text{AsPh}_3)_2\text{I}_2$	2.558 (85.3%)	27	a
$\text{Co}(\text{PPh}_3)_2\text{Br}_2$	2.570 (85.7%)	13.83(2)	84
$\text{Co}(\text{PPh}_3)_2\text{Cl}_2$	2.585 (86.2%)	14.89(2)	84
Co-MST-H_2O	2.627 (87.6%)	25.3	Current work
Co-TODA (CP)	2.68-2.69 (89.3%-89.7%)	40.2	46
$\text{Co}(\text{acac})_2(\text{H}_2\text{O})_2$	2.81 (93.7%)	57.0	153
$[\text{Co}(12\text{-crown-4})_2](\text{I}_3)_2$	2.82 (94.0%)	24.7	a

^a SMM behaviors of $[\text{Co}(12\text{-crown-4})_2](\text{I}_3)_2$ and $\text{Co}(\text{AsPh}_3)_2\text{I}_2$ were probed by Saber and Dunbar in ref. 154 and by Chen et al. in ref. 155, respectively. Their D' values determined by advanced spectroscopies were reported in refs. 47 and 123, respectively. Spin densities of $[\text{Co}(12\text{-crown-}$

4)₂](I₃)₂ and Co(AsPh₃)₂I₂ have been calculated and are reported here for comparison. Tables listing the spin densities for these complexes are given in Tables S3-S6.

Hirshfeld surface analysis

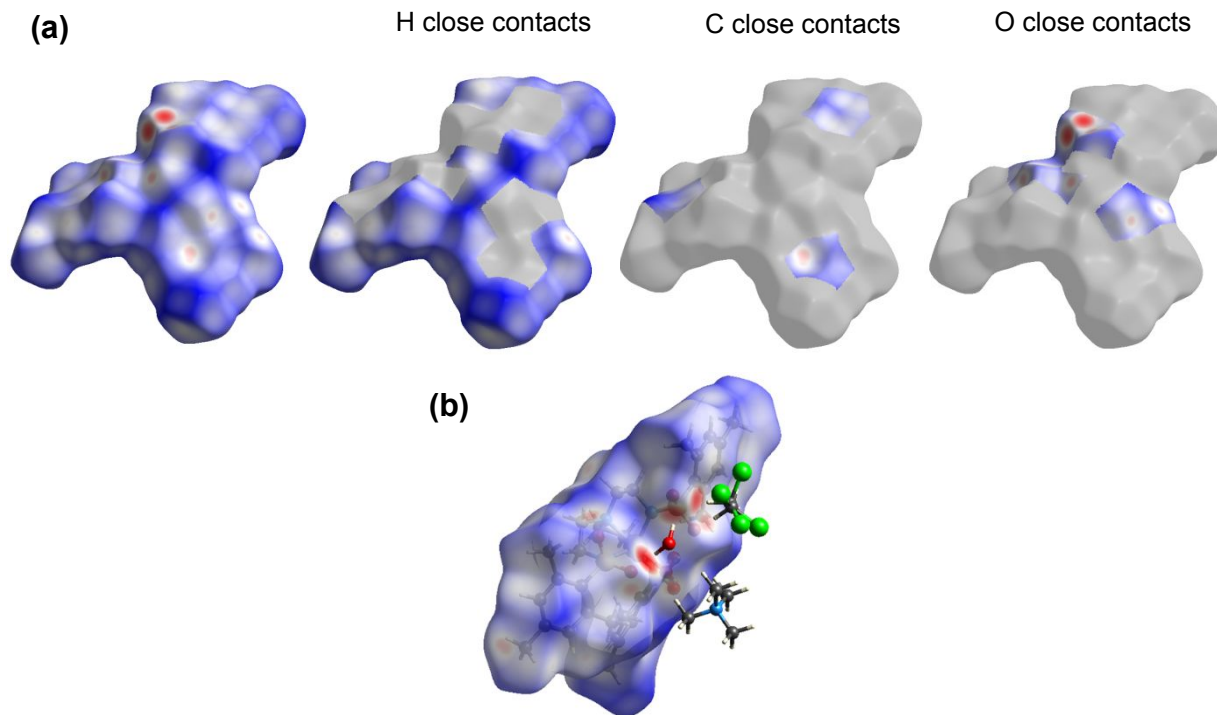
Hirshfeld surface analysis^{121, 125} is especially effective to examine which parts of a molecule interact most strongly with neighboring molecules in the crystal solid.^{68, 126-148} A Hirshfeld surface is an isosurface calculated from the weight function $w(\mathbf{r})$ of the sum of spherical atom electron densities (Eq. 6):

$$w(\mathbf{r}) = \frac{\rho_{promolecule}(\mathbf{r})}{\rho_{procrystal}(\mathbf{r})} = \frac{\sum_{A \in molecule} \rho_A(\mathbf{r})}{\sum_{A \in crystal} \rho_A(\mathbf{r})} \quad (6)$$

where $\rho_{promolecule}(\mathbf{r})$ is the sum of the molecular electron density over the atoms in the molecule or ions under consideration (the promolecule) and $\rho_{procrystal}(\mathbf{r})$ is the similar sum over the crystal (the procrystal).^{121, 125}

The isosurface here separates a molecule (promolecule) or ion from its nearest neighbors (procrystal) at a given density level. Distances to the nearest atoms outside (external), d_e , and inside (internal), d_i , are defined from the Hirshfeld surface, giving a 3-*D* representation of the intermolecular, close contacts in the crystal using the *CrystalExplorer* software by Spackman and coworkers at the University of Western Australia.^{121, 125} Also, the Hirshfeld surface could be made into a 2-*D* histogram with a unique fingerprint plot for intermolecular interactions.

Surfaces (Figure 6) and fingerprint plots (Figure S12) for the [Co(MST)(OH₂)]⁻ anion (named **Co-MST-H₂O**⁻) show interactions with neighboring molecules, cation Me₄N⁺, and lattice solvents (CH₂Cl₂ and H₂O), while the average surface reveals low to moderate intensity. The strongest interactions are from those of the O atoms of the sulfonyl groups interacting with solvents in the lattice (CH₂Cl₂ and H₂O through hydrogen bonds), as shown by the red spots in Figure 6b. The interactions of the anion with the cation NMe₄⁺ are present but not strong, as there are no nearby red spots near NMe₄⁺ in Figure 6b. Interactions of H atoms with other **Co-MST-H₂O** molecules, the solvents, and the cation NMe₄⁺ take the largest share (83.9%) of close interactions with neighboring molecules, as shown in Table 3.



26
27
28
29
30
31
32
33
34
35
36
37
38

Figure 6. (a) Hirshfeld surfaces of the **Co-MST-H₂O⁻** ion showing surface interactions as heat maps. Red zones indicate strong interactions with closer distances between d_e and d_i atoms, while blue zones are indicative of larger distances and less strong interactions. (b) Representations of the closest and more intense interactions of the **Co-MST-H₂O⁻** Hirshfeld surface, showing that lattice H₂O forms hydrogen bonds with the O atoms in the MST³⁻ ligand. The H atoms of lattice CH₂Cl₂ also interact fairly strongly with O atoms of ligand. The CH₂Cl₂ molecule is disordered.

39
40
41
42
43

Table 3. Hirshfeld surface coverage based on interactions of atoms on the **M-MST⁻** anion with all nearby atoms of neighboring molecules and Me₄N⁺ cation. Most of the interactions are from H atoms of the **M-MST⁻** anion with surrounding atoms.

44
45
46
47
48
49
50
51
52
53
54
55
56
57

	Co-MST-H₂O	Ni-MST-H₂O
H close contacts	83.9%	79.7%
C close contacts	8.6%	9.8%
O close contacts	7.5%	10.5%
N close contacts	>0.1%	>0.1%
S close contacts	>0.1%	>0.1%
M close contacts	>0.1%	>0.1%

[NMe₄][Ni(MST)(OH₂)] (Ni-MST-H₂O)

Phonon properties of **Ni-MST-H₂O** have been studied by INS, DFT-phonon calculations, and Hirschfeld surface analysis. HFEPR was not used for **Ni-MST-H₂O** as the effective range for HFEPR using current instrumentation is up to ~ 30 cm⁻¹, while the expected transition from previously reported magnetometry is near 209 cm⁻¹.⁵⁷ Repeated attempts to probe powder samples of **Ni-MST-H₂O** by FIRMS (Figure S13) did not show any magnetic peaks. VT INS spectra of powder samples in Figure 7 also did not clearly reveal magnetic peaks in the spectra. VT profile of the shoulder peak at ~ 208 cm⁻¹ indicates that it is mostly phonon in nature with possible magnetic contributions to the intensity. Both FIRMS and INS spectra show strong, broad phonon peaks at ~ 210 cm⁻¹. We speculate that the following may lead to the results in the current studies: (1) The magnetic transitions among the ZFS states in Figure 1d are possibly too weak to be observed by both FIRMS and INS; (2) The magnetic transitions undergo spin-phonon couplings with the nearby strong phonons, dividing the magnetic features over several phonons, making the direct observation of the magnetic transition difficult. For future spectroscopic studies, the use of single crystals in FIRMS and deuterated **Ni-MST-H₂O** samples in VT INS is expected to help revealing magnetic transitions in **Ni-MST-H₂O**.

Earlier, Schulte, Vignesh, and Dunbar determined spin-Hamiltonian parameters of **Ni-MST-H₂O** using DC magnetic susceptibility and reduced magnetization.⁵⁷ The current results suggest that the magnetometry remains the only viable technique to determine spin-Hamiltonian parameters for **Ni-MST-H₂O**. We have thus focused on the phonon properties of **Ni-MST-H₂O** revealed by INS, DFT phonon calculations, and Hirshfeld surface analysis.

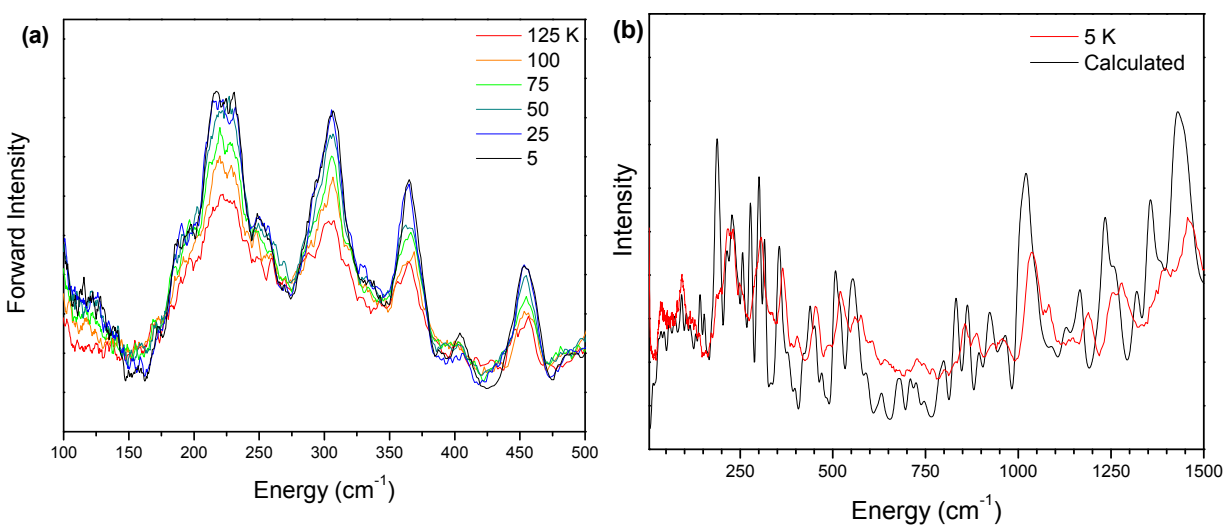
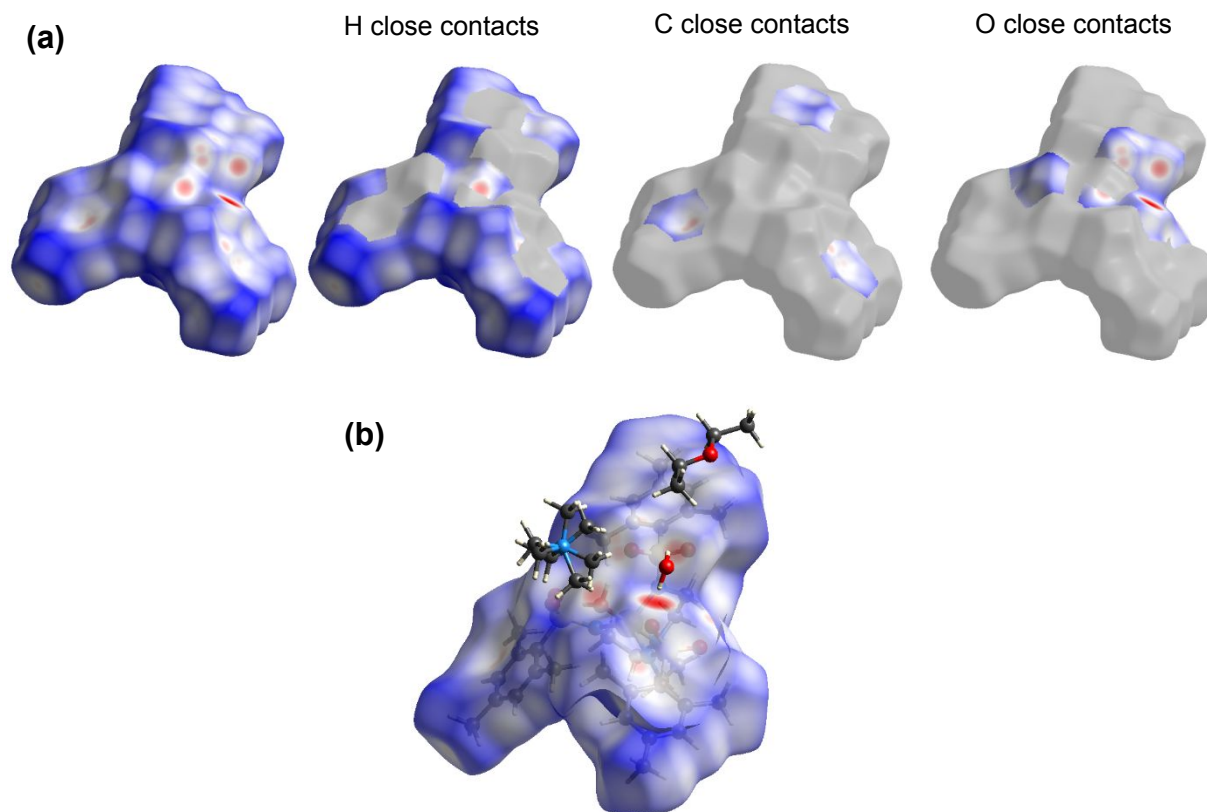


Figure 7. (a) Bose-corrected INS spectra of **Ni-MST-H₂O** from 100-500 cm⁻¹. There are no

1
2
3 strong magnetic features in this region. (b) INS spectra showing calculated and experimental
4 phonons at 5–1500 cm^{-1} of **Ni-MST-H₂O**. Additional regions of the experimental and calculated
5 INS are given in Figures S16-S18.
6
7

8
9 INS spectra of **Ni-MST-H₂O** are given in Figure 7. DFT calculated INS spectrum is given
10 in Figure 7b in comparison with the experimental INS spectrum, showing a good fit between the
11 two spectra.
12
13

14 Surfaces (Figure 8) and fingerprint plots (Figure S19) for the $[\text{Ni}(\text{MST})(\text{OH}_2)]^-$ anion
15 (named **Ni-MST-H₂O⁻**) show intense interactions between the anion and the lattice solvent H_2O
16 (through hydrogen bonds) and the cation Me_4N^+ through the O atoms of the sulfonyl groups, as
17 shown by the red spots in Figure 8b. In comparison, the interactions between **Co-MST-H₂O⁻**
18 and its cation NMe_4^+ are not as strong, as discussed earlier and shown in Figure 6b. The
19 interactions of the anion with the other solvent, ethyl ether Et_2O , are present but not strong, as
20 there are no nearby red spots around Et_2O in Figure 8b. Interactions of H atoms with other **Ni-**
21 **MST-H₂O** molecules, the solvents, and the cation NMe_4^+ take the largest share (79.7%) of close
22 interactions with neighboring molecules, as shown in Table 3.
23
24
25
26
27
28
29
30
31
32
33
34
35
36
37
38
39
40
41
42
43
44
45
46
47
48
49
50
51
52
53
54
55
56
57
58
59
60



31 **Figure 8.** (a) Hirshfeld surfaces of the **Ni-MST-H₂O⁻** anion showing surface interactions as heat
32 maps. Red zones indicate strong interactions with closer distances between d_e and d_i atoms,
33 while blue zones are indicative of larger distances and less strong interactions. (b)
34 Representations of the closest and more intense interactions of the **Ni-MST-H₂O⁻** Hirschfeld
35 surface, showing that H₂O solvent molecule and the Me₄N⁺ cation form hydrogen bonds with the
36 O atoms in the MST³⁻ ligand. The ethyl ether Et₂O solvent molecule, in contrast, does not show
37 strong interactions with the **Ni-MST-H₂O⁻** anion. The Me₄N⁺ cation is disordered.

38 Conclusions

39 In this work, the use of advanced spectroscopies to probe magnetic transitions in **Co-**
40 **MST-H₂O** has delivered spin-Hamiltonian parameters for that compound. INS studies also give
41 phonon properties of the complex. DFT phonon calculations give calculated INS spectrum that
42 fits well with the experimental INS spectrum. The calculations also determined phonon
43 symmetries, their energies, and phonon movies. In addition, the DFT phonon calculations yield
44 spin density on the Co²⁺ ion and other atoms in **Co-MST-H₂O**. Hirshfeld surface analysis reveals
45 how the **Co-MST-H₂O⁻** anion interacts with its cation, solvent molecules, and neighboring **Co-**
46

MST-H₂O molecules. For **Ni-MST-H₂O**, phonon properties and intermolecular interactions have been studied by INS, DFT phonon calculations, and Hirshfeld surface analysis. FIRMS and INS studies of **Ni-MST-H₂O** did not show its magnetic transitions. Thus, the current work on **Co-MST-H₂O** offers a very good comparison (between results from magnetometry and spectroscopic techniques). For **Ni-MST-H₂O**, magnetometry is the viable technique to determine spin-Hamiltonian parameters for the compound in the absence of magnetic resonance or INS results.

Experimental

Synthesis

Synthesis of the H₃MST ligand was completed using commercial materials with no further purification following a reported procedure.¹⁵⁶ **Co-MST-H₂O** and **Ni-MST-H₂O** were prepared following reported procedures.^{57, 78}

FIRMS

Far-IR magneto-spectroscopy was completed at the National High Magnetic Field Laboratory in Tallahassee Florida using a Bruker Vertex 80v Fourier-transform infrared (FT-IR) spectrometer coupled with a 17.5 T, vertical-bore superconducting magnet. The experimental setup is equipped with a mercury lamp and a composite silicon bolometer (Infrared Laboratories), as an incoherent (sub)-THz radiation source and detector, respectively. The THz radiation propagates in freespace inside the optical beamline, connecting the output of the spectrometer and top of the sample probe. The radiation then passes through the brass light-pipe through a 2.5 m distance to the field center. The probe and beamline are evacuated to eliminate strong parasitic absorptions of the air. Samples were prepared by mixing with eicosane under a heat lamp to make a slurry, making a solid layer of polycrystalline sample. Measurements were conducted at 5 K with the sample and bolometer being cooled by low pressure He gas. Spectrum transmitted through the samples was collected between 10 and 720 cm⁻¹ with a resolution of 0.3 cm⁻¹.

HFEP R

HFEP R spectra were collected at the National High Magnetic Field Laboratory in the EMR facility using a spectrometer previously described,¹⁵⁷ modified with the use of VDI sources. The spectrometer is associated with a 15/17 T warm-bore superconducting magnet. **Co-MST-**

1
2
3 **H₂O** was measured both “as is” and as a pellet pressed with *n*-eicosane to prevent torquing
4 effects of the sample in the magnetic field.
5
6
7

8 **Inelastic neutron scattering (INS)**

9 Variable-temperature INS spectra was collected at Oak Ridge National Laboratory using
10 VISION, an indirect-geometry vibrational spectrometer.¹⁰³ About 500 mg of sample was used for
11 data collection, sealed in a vanadium can within a helium environment. VISION has two detector
12 banks; magnetic transitions are more intense in the forward scattering detectors for their low
13 scattering angle dependence.
14
15
16
17
18

19 **Phonon and INS calculations**

20 DFT calculations were performed using the Vienna Ab initio Simulation Package
21 (VASP).¹⁵⁸ Lattice parameters and atomic coordinates from published structures were used for
22 the structure. Atomic force constants were calculated by VASP using finite displacement
23 method, and vibrational eigen-frequencies and modes were calculated using Phonopy and
24 OCLIMAX software was used to convert DFT calculated phonon results to the simulated INS
25 spectra.¹⁵⁹⁻¹⁶⁴
26
27
28
29
30
31

32 **Hirschfeld surface analysis**

33 Surfaces were generated using Crystal Explorer.^{121, 125} Surfaces for this analysis were
34 generated from reported structures.⁵⁷ Only atoms within the SMM complex were selected to
35 allow for determination of interactions with counter ions and nearby SMM complexes within the
36 crystal structure. Charges for the metal complexes in **Co-MST-H₂O** and **Ni-MST-H₂O** were set
37 to -1 while the NMe₄ counter ion was set to +1.
38
39
40
41
42

43 **Associate Content**

44 ESI including powder X-ray diffraction data of the samples, additional FIRMS, HFEPR,
45 and INS results, additional Hirschfeld surfaces and fingerprint plots, and spin densities. Phonon
46 movies of the anion in **Co-MST-H₂O**.
47
48
49

50 **Notes**

51 The authors declare no competing financial interest.
52
53
54
55
56
57

Acknowledgements

US National Science Foundation (CHE-2055499 and CHE-2349345) for financial support of this research. Part of this work was performed at the National High Magnetic Field Laboratory which is supported by NSF Cooperative Agreement No. DMR-2128556 and the State of Florida. Neutron scattering experiments were conducted at the Spallation Neutron Source, which is supported by the Scientific Users Facilities Division, Office of Basic Energy Sciences, U.S. Department of Energy under Contract DE-AC0500OR22725 with UT Battelle, LLC. This research used computing resources made available through the VirtuES and the ICE-MAN projects, funded by Laboratory Directed Research and Development program and Compute and Data Environment for Science (CADES) at ORNL, as well as resources of National Energy Research Scientific Computing Center (NERSC), a U.S. Department of Energy Office of Science User Facility located at Lawrence Berkeley National Laboratory, operated under Contract No. DE-AC02-05CH11231 using NERSC award ERCAP0024340. The authors thank Adam T. Hand for assistance with FIRMS analysis and Dr. Andrew Ozarowski for his EPR simulation program SPIN.

References

1. M. N. Leuenberger and D. Loss, Quantum computing in molecular magnets. *Nature*, 2001, **410**, 789-793. <https://doi.org/10.1038/35071024>.
2. D. Aravena and E. Ruiz, Spin dynamics in single-molecule magnets and molecular qubits. *Dalton Trans.*, 2020, **49**, 9916-9928. <https://doi.org/10.1039/D0DT01414A>.
3. J. M. Frost, K. L. M. Harriman and M. Murugesu, The rise of 3-d single-ion magnets in molecular magnetism: towards materials from molecules? *Chem. Sci.*, 2016, **7**, 2470-2491. <https://doi.org/10.1039/C5SC03224E>.
4. A. Zabala-Lekuona, J. M. Seco and E. Colacio, Single-Molecule Magnets: From Mn₁₂-ac to dysprosium metallocenes, a travel in time. *Coord. Chem. Rev.*, 2021, **441**, 213984. <https://doi.org/10.1016/j.ccr.2021.213984>.
5. L. Bogani and W. Wernsdorfer, Molecular spintronics using single-molecule magnets. *Nat. Mater.*, 2008, **7**, 179-186. <https://doi.org/10.1038/nmat2133>.
6. A. R. Rocha, V. M. Garcia-Suarez, S. W. Bailey, C. J. Lambert, J. Ferrer and S. Sanvito, Towards molecular spintronics. *Nat. Mater.*, 2005, **4**, 335-339. <https://doi.org/10.1038/nmat1349>.

- 1
2
3 7. S. Sanvito and A. R. Rocha, Molecular-spintronics: The art of driving spin through
4 molecules. *J. Comput. Theor. Nanosci.*, 2006, **3**, 624-642.
5
6 <https://doi.org/10.1166/jctn.2006.3047>.
7
- 8 8. A. Soncini and L. F. Chibotaru, Molecular spintronics using noncollinear magnetic
9 molecules. *Phys. Rev. B*, 2010, **81**, 132403.
10
11 <https://doi.org/10.1103/PhysRevB.81.132403>.
12
- 13 9. K. C. Nowack, F. H. L. Koppens, Y. V. Nazarov and L. M. K. Vandersypen, Coherent
14 control of a single electron spin with electric fields. *Science*, 2007, **318**, 1430-1433.
15
16 <https://doi.org/10.1126/science.1148092>.
17
- 18 10. A. K. Bar, C. Pichon and J.-P. Sutter, Magnetic Anisotropy in Two- to Eight-Coordinated
19 Transition-Metal Complexes: Recent Developments in Molecular Magnetism. *Coord.*
20 *Chem. Rev.*, 2016, **308**, 346-380. <https://doi.org/10.1016/j.ccr.2015.06.013>.
21
- 22 11. C. Benelli and D. Gatteschi, *Introduction to Molecular Magnetism: From Transition*
23 *Metals to Lanthanides*, John Wiley & Sons, 2015.
24
- 25 12. S. Gao, *Molecular Nanomagnets and Related Phenomena*, 2015.
26
27 <http://doi.org/10.1007/978-3-662-45723-8>.
28
- 29 13. D. Gatteschi, R. Sessoli and J. Villain, *Molecular Nanomagnets*, Oxford University Press,
30 New York, 2006. <https://doi.org/10.1093/acprof:oso/9780198567530.001.0001>.
31
- 32 14. R. E. P. Winpenny, Quantum Information Processing Using Molecular Nanomagnets As
33 Qubits. *Angew. Chem. Int. Ed.*, 2008, **47**, 7992-7994.
34
35 <https://doi.org/10.1002/anie.200802742>.
36
- 37 15. M. Holynska, *Single-Molecule Magnets: Molecular Architectures and Building Blocks for*
38 *Spintronics*, Wiley-VCH, Weinheim, Germany, 2019.
39
40 <https://doi.org/10.1002/9783527809929>.
41
- 42 16. P. S. Perlepe, D. Maniaki, E. Pilichos, E. Katsoulakou and S. P. Perlepes, Smart
43 Ligands for Efficient 3d-, 4d- and 5d-Metal Single-Molecule Magnets and Single-Ion
44 Magnets. *Inorganics*, 2020, **8**, 39. <https://doi.org/10.3390/inorganics8060039>.
45
- 46 17. D. Shao and X.-Y. Wang, Development of Single-Molecule Magnets. *Chin. J. Chem.*,
47 2020, **38**, 1005-1018. <https://doi.org/10.1002/cjoc.202000090>.
48
- 49 18. E. Collet, Ultrafast control of anisotropy. *Nat. Chem.*, 2020, **12**, 429-430.
50
51 <https://doi.org/10.1038/s41557-020-0462-z>.
52
- 53 19. M. Feng and M.-L. Tong, Single Ion Magnets from 3d to 5f: Developments and
54 Strategies. *Chem. Eur. J.*, 2018, **24**, 7574-7594.
55
56 <https://doi.org/10.1002/chem.201705761>.
57

- 1
2
3 20. R. Ruamps, R. Maurice, L. Batchelor, M. Boggio-Pasqua, R. Guillot, A. L. Barra, J. Liu,
4 E.-E. Bendeif, S. Pillet, S. Hill, T. Mallah and N. Guihéry, Giant Ising-Type Magnetic
5 Anisotropy in Trigonal Bipyramidal Ni(II) Complexes: Experiment and Theory. *J. Am.*
6 *Chem. Soc.*, 2013, **135**, 3017-3026. <https://doi.org/10.1021/ja308146e>.
7
8 21. R. Sessoli, D. Gatteschi, A. Caneschi and M. A. Novak, Magnetic bistability in a metal-
9 ion cluster. *Nature*, 1993, **365**, 141-143. <https://doi.org/10.1038/365141a0>.
10
11 22. A. Świtlicka, B. Machura, J. Cano, F. Lloret and M. Julve, A Study of the Lack of Slow
12 Magnetic Relaxation in Mononuclear Trigonal Bipyramidal Cobalt (II) Complexes.
13 *ChemistrySelect*, 2021, **6**, 576-582. <https://doi.org/10.1002/slct.202100061>.
14
15 23. C. A. P. Goodwin, Blocking like it's hot: a synthetic chemists' path to high-temperature
16 lanthanide single molecule magnets. *Dalton Trans.*, 2020, **49**, 14320-14337.
17 <https://doi.org/10.1039/D0DT01904F>.
18
19 24. A. Sarkar, S. Dey and G. Rajaraman, Role of Coordination Number and Geometry in
20 Controlling the Magnetic Anisotropy in Fe^{II}, Co^{II}, and Ni^{II} Single-Ion Magnets. *Chem. Eur.*
21 *J.*, 2020, **26**, 14036-14058. <https://doi.org/10.1002/chem.202003211>.
22
23 25. S. E. Stavretis, Y. Cheng, L. L. Daemen, C. M. Brown, D. H. Moseley, E. Bill, M.
24 Atanasov, A. J. Ramirez-Cuesta, F. Neese and Z. L. Xue, Probing Magnetic Excitations
25 in Co^{II} Single-Molecule Magnets by Inelastic Neutron Scattering. *Eur. J. Inorg. Chem.*,
26 2019, **2019**, 1119-1127. <https://doi.org/10.1002/ejic.201801088>.
27
28 26. H.-H. Cui, M.-M. Ding, X.-D. Zhang, W. Lv, Y.-Q. Zhang, X.-T. Chen, Z. Wang, Z.-W.
29 Ouyang and Z.-L. Xue, Magnetic anisotropy in square pyramidal cobalt(II) complexes
30 supported by a tetraazo macrocyclic ligand. *Dalton Trans.*, 2020, **49**, 14837-14846.
31 <http://doi.org/10.1039/D0DT01954B>.
32
33 27. Z.-B. Hu, X. Feng, J. Li, Y.-Q. Zhang, L. Yin, Z. Wang, Z. Ouyang, M. Kurmoo and Y.
34 Song, Optimal diamagnetic dilution concentration for suppressing the dipole–dipole
35 interaction in single-ion magnets. *Dalton Trans.*, 2020, **49**, 2159-2167.
36 <http://doi.org/10.1039/C9DT04403E>.
37
38 28. M. A. Hay, A. Sarkar, G. A. Craig, K. E. R. Marriott, C. Wilson, G. Rajaraman and M.
39 Murrie, A large axial magnetic anisotropy in trigonal bipyramidal Fe(II). *Chem. Commun.*,
40 2020, **56**, 6826-6829. <http://dx.doi.org/10.1039/D0CC02382E>.
41
42 29. P. Kumar, D. J. SantaLucia, K. Kaniewska-Laskowska, S. V. Lindeman, A. Ozarowski, J.
43 Krzystek, M. Ozerov, J. Telsler, J. F. Berry and A. T. Fiedler, Probing the Magnetic
44 Anisotropy of Co(II) Complexes Featuring Redox-Active Ligands. *Inorg. Chem.*, 2020,
45 **59**, 16178-16193. <https://doi.org/10.1021/acs.inorgchem.0c01812>.
46
47
48
49
50
51
52
53
54
55
56
57
58
59
60

- 1
2
3 30. M. Liu, Y. Yang, R. Jing, S. Zheng, A. Yuan, Z. Wang, S.-C. Luo, X. Liu, H.-H. Cui, Z.-W.
4 Ouyang and L. Chen, Slow magnetic relaxation in dinuclear Co(III)–Co(II) complexes
5 containing a five-coordinated Co(II) centre with easy-axis anisotropy. *Dalton Trans.*,
6 2022, **51**, 8382-8389. <http://doi.org/10.1039/D2DT00857B>.
7
8
9 31. W. Lv, H.-H. Cui, L. Chen, Y.-Q. Zhang, X.-T. Chen, Z. Wang, Z.-W. Ouyang and Z.-L.
10 Xue, Magnetic anisotropy of two tetrahedral Co(II)-halide complexes with
11 triphenylphosphine ligands. *Dalton Trans.*, 2022, **51**, 7530-7538.
12
13 <http://doi.org/10.1039/D2DT00121G>.
14
15 32. S. Gopal Patra and P. Kumar Chattaraj, Three coordinated first row-transition metal
16 complexes, $[M\{N(SiMe_3)_2\}_3]-1/0$: Structure, bonding, and magnetic properties.
17 *Polyhedron*, 2024, **256**, 116990. <https://doi.org/10.1016/j.poly.2024.116990>.
18
19 33. M. A. Hay, A. Sarkar, G. A. Craig, L. Bhaskaran, J. Nehrkorn, M. Ozerov, K. E. R.
20 Marriott, C. Wilson, G. Rajaraman, S. Hill and M. Murrie, In-depth investigation of large
21 axial magnetic anisotropy in monometallic 3d complexes using frequency domain
22 magnetic resonance and ab initio methods: a study of trigonal bipyramidal Co(II). *Chem.*
23 *Sci.*, 2019, **10**, 6354-6361. <http://doi.org/10.1039/C9SC00987F>.
24
25 34. M. A. Hay, C. J. McMonagle, C. Wilson, M. R. Probert and M. Murrie, Trigonal to
26 Pentagonal Bipyramidal Coordination Switching in a Co(II) Single-Ion Magnet. *Inorg.*
27 *Chem.*, 2019, **58**, 9691-9697. <https://doi.org/10.1021/acs.inorgchem.9b00515>.
28
29 35. C. D. Hastings, L. S. X. Huffman, C. K. Tiwari, J. G. Betancourth, W. W. Brennessel and
30 B. R. Barnett, Coordinatively Unsaturated Metallates of Cobalt(II), Nickel(II), and Zinc(II)
31 Guarded by a Rigid and Narrow Void. *Inorg. Chem.*, 2023, **62**, 11920-11931.
32
33 <https://doi.org/10.1021/acs.inorgchem.3c01335>.
34
35 36. A. L. Nagelski, M. Ozerov, M. S. Fataftah, J. Krzystek, S. M. Greer, P. L. Holland and J.
36 Telser, Electronic Structure of Three-Coordinate FeII and CoII β -Diketimate
37 Complexes. *Inorg. Chem.*, 2024, **63**, 4511-4526.
38
39 <https://doi.org/10.1021/acs.inorgchem.3c03388>.
40
41 37. R. Boča, Zero-Field Splitting in Metal Complexes. *Coord. Chem. Rev.*, 2004, **248**, 757-
42 815. <https://doi.org/10.1016/j.ccr.2004.03.001>.
43
44 38. K. N. Shrivastava, Theory of Spin–Lattice Relaxation. *Phys. Stat. Sol. (b)*, 1983, **117**,
45 437-458. <https://doi.org/10.1002/pssb.2221170202>.
46
47 39. J. R. Pilbrow, Effective g values for $S = 3/2$ and $S = 5/2$. *J. Magn. Reson.*, 1978, **31**, 479-
48 490. [https://doi.org/10.1016/S0022-2364\(78\)80015-8](https://doi.org/10.1016/S0022-2364(78)80015-8).
49
50
51
52
53
54
55
56
57
58
59
60

- 1
2
3
4
5
6
7
8
9
10
11
12
13
14
15
16
17
18
19
20
21
22
23
24
25
26
27
28
29
30
31
32
33
34
35
36
37
38
39
40
41
42
43
44
45
46
47
48
49
50
51
52
53
54
55
56
57
58
59
60
40. R. Boča, L. u. Dlháň, W. Linert, H. Ehrenberg, H. Fuess and W. Haase, Ligand sphere-enhanced magnetic anisotropy in cobalt(II) and manganese(II) 2,6-bis-(benzimidazol-2'-yl)-pyridine dichloride. *Chem. Phys. Lett.*, 1999, **307**, 359-366.
[https://doi.org/10.1016/S0009-2614\(99\)00519-9](https://doi.org/10.1016/S0009-2614(99)00519-9).
41. C. Rajnák, J. Titiš, I. Šalitroš, R. Boča, O. Fuhr and M. Ruben, Zero-field splitting in pentacoordinate Co(II) complexes. *Polyhedron*, 2013, **65**, 122-128.
<https://doi.org/10.1016/j.poly.2013.08.029>.
42. L. Smolko, J. Černák, J. Kuchár, C. Rajnák, J. Titiš and R. Boča, Field-Induced Slow Magnetic Relaxation in Mononuclear Tetracoordinate Cobalt(II) Complexes Containing a Neocuproine Ligand. *Eur. J. Inorg. Chem.*, 2017, **2017**, 3080-3086.
<https://doi.org/10.1002/ejic.201700293>.
43. X. Hou, X. Wang, X. Liu, J. Wang, L. Tang and P. Ju, Fine-tuning the effects of auxiliary ligands on two trigonal-bipyramid cobalt(ii) complexes exhibiting field-induced slow magnetic relaxation. *New J. Chem.*, 2018, **42**, 8583-8590.
<http://doi.org/10.1039/C8NJ01201F>.
44. O. Stetsiuk, A. El-Ghayoury, F. Lloret, M. Julve and N. Avarvari, Mononuclear and One-Dimensional Cobalt(II) Complexes with the 3,6-Bis(picolylamino)-1,2,4,5-tetrazine Ligand. *Eur. J. Inorg. Chem.*, 2018, **2018**, 449-457.
<https://doi.org/10.1002/ejic.201701224>.
45. F. Shao, B. Cahier, Y.-T. Wang, F.-L. Yang, E. Rivière, R. Guillot, N. Guihéry, J.-P. Tong and T. Mallah, Magnetic Relaxation Studies on Trigonal Bipyramidal Cobalt(II) Complexes. *Chem. Asian J.*, 2020, **15**, 391-397. <https://doi.org/10.1002/asia.201901511>.
46. P. Tin, A. N. Bone, N. N. Bui, Y.-Q. Zhang, T. Chang, D. H. Moseley, M. Ozerov, J. Krzystek, Y. Cheng, L. L. Daemen, X. Wang, L. Song, Y.-S. Chen, D. Shao, X.-Y. Wang, X.-T. Chen and Z.-L. Xue, Advanced Spectroscopic and Computational Studies of a Cobalt(II) Coordination Polymer with Single-Ion-Magnet Properties. *J. Phys. Chem. C*, 2022, **126**, 13268-13283. <https://doi.org/10.1021/acs.jpcc.2c03083>.
47. D. H. Moseley, Z. Liu, A. N. Bone, S. E. Stavretis, S. K. Singh, M. Atanasov, Z. Lu, M. Ozerov, K. Thirunavukkuarasu, Y. Cheng, L. L. Daemen, D. Lubert-Perquel, D. Smirnov, F. Neese, A. J. Ramirez-Cuesta, S. Hill, K. R. Dunbar and Z.-L. Xue, Comprehensive Studies of Magnetic Transitions and Spin-Phonon Couplings in the Tetrahedral Cobalt Complex Co(AsPh₃)₂I₂. *Inorg. Chem.*, 2022, **61**, 17123-17136.
<https://doi.org/10.1021/acs.inorgchem.2c02604>.

- 1
2
3
4
5
6
7
8
9
10
11
12
13
14
15
16
17
18
19
20
21
22
23
24
25
26
27
28
29
30
31
32
33
34
35
36
37
38
39
40
41
42
43
44
45
46
47
48
49
50
51
52
53
54
55
56
57
58
59
60
48. T. Jurca, A. Farghal, P.-H. Lin, I. Korobkov, M. Murugesu and D. S. Richeson, Single-Molecule Magnet Behavior with a Single Metal Center Enhanced through Peripheral Ligand Modifications. *J. Am. Chem. Soc.*, 2011, **133**, 15814-15817. <https://doi.org/10.1021/ja204562m>.
49. R. Ruamps, L. J. Batchelor, R. Guillot, G. Zakhia, A.-L. Barra, W. Wernsdorfer, N. Guihéry and T. Mallah, Ising-type magnetic anisotropy and single molecule magnet behaviour in mononuclear trigonal bipyramidal Co(II) complexes. *Chem. Sci.*, 2014, **5**, 3418-3424. <http://doi.org/10.1039/C4SC00984C>.
50. B. Cahier, R. Maurice, H. Bolvin, T. Mallah and N. Guihéry, Tools for Predicting the Nature and Magnitude of Magnetic Anisotropy in Transition Metal Complexes: Application to Co(II) Complexes. *Magnetochemistry*, 2016, **2**, 31. <https://doi.org/10.3390/magnetochemistry2030031>.
51. A. K. Mondal, J. Jover, E. Ruiz and S. Konar, Investigation of easy-plane magnetic anisotropy in P-ligand square-pyramidal Co(II) single ion magnets. *Chem. Commun.*, 2017, **53**, 5338-5341. <http://doi.org/10.1039/C7CC02584J>.
52. J. Acharya, A. Sarkar, P. Kumar, V. Kumar, J. Flores Gonzalez, O. Cador, F. Pointillart, G. Rajaraman and V. Chandrasekhar, Influence of ligand field on magnetic anisotropy in a family of pentacoordinate Co(II) complexes. *Dalton Trans.*, 2020, **49**, 4785-4796. <http://doi.org/10.1039/D0DT00315H>.
53. F. Shao, B. Cahier, E. Rivière, R. Guillot, N. Guihéry, V. E. Campbell and T. Mallah, Structural Dependence of the Ising-type Magnetic Anisotropy and of the Relaxation Time in Mononuclear Trigonal Bipyramidal Co(II) Single Molecule Magnets. *Inorg. Chem.*, 2017, **56**, 1104-1111. <https://doi.org/10.1021/acs.inorgchem.6b01966>.
54. J. Krzystek, D. C. Swenson, S. A. Zvyagin, D. Smirnov, A. Ozarowski and J. Telsner, Cobalt(II) "Scorpionate" Complexes as Models for Cobalt-Substituted Zinc Enzymes: Electronic Structure Investigation by High-Frequency and -Field Electron Paramagnetic Resonance Spectroscopy. *J. Am. Chem. Soc.*, 2010, **132**, 5241-5253. <https://doi.org/10.1021/ja910766w>.
55. E. J. L. McInnes and R. E. P. Winpenny, *Molecular Magnets*, in *Comp. Inorg. Chem. II*, ed. K. Poeppelmeier, Elsevier, Amsterdam, 2013. <https://doi.org/10.1016/B978-0-08-097774-4.00419-8>.
56. D. G. McGavin, Symmetry constraints on EPR spin-Hamiltonian parameters. *J. Magn. Reson.*, 1987, **74**, 19-55. [https://doi.org/10.1016/0022-2364\(87\)90077-1](https://doi.org/10.1016/0022-2364(87)90077-1).

- 1
2
3 57. K. A. Schulte, K. R. Vignesh and K. R. Dunbar, Effects of coordination sphere on
4 unusually large zero field splitting and slow magnetic relaxation in trigonally symmetric
5 molecules. *Chem. Sci.*, 2018, **9**, 9018-9026. <https://doi.org/10.1039/C8SC02820F>.
6
7
8 58. F. Shao, B. Cahier, N. Guihéry, E. Rivière, R. Guillot, A.-L. Barra, Y. Lan, W.
9 Wernsdorfer, V. E. Campbell and T. Mallah, Tuning the Ising-type anisotropy in trigonal
10 bipyramidal Co(II) complexes. *Chem. Commun.*, 2015, **51**, 16475-16478.
11
12 <http://doi.org/10.1039/C5CC07741A>.
13
14 59. D. Schweinfurth, M. G. Sommer, M. Atanasov, S. Demeshko, S. Hohloch, F. Meyer, F.
15 Neese and B. Sarkar, The Ligand Field of the Azido Ligand: Insights into Bonding
16 Parameters and Magnetic Anisotropy in a Co(II)-Azido Complex. *J. Am. Chem. Soc.*,
17 2015, **137**, 1993-2005. <https://doi.org/10.1021/ja512232f>.
18
19 60. H.-H. Cui, H. Xu, M. Zhang, S. Luo, W. Tong, M. Wang, T. Sun, L. Chen and Y. Tang,
20 Magnetic Anisotropy from Easy-Plane to Easy-Axial in Square Pyramidal Cobalt(II)
21 Single-Ion Magnets. *Cryst. Growth Des.*, 2022, **22**, 2742-2748.
22
23 <https://doi.org/10.1021/acs.cgd.2c00160>.
24
25 61. F. Habib, O. R. Luca, V. Vieru, M. Shiddiq, I. Korobkov, S. I. Gorelsky, M. K. Takase, L.
26 F. Chibotaru, S. Hill, R. H. Crabtree and M. Murugesu, Influence of the Ligand Field on
27 Slow Magnetization Relaxation versus Spin Crossover in Mononuclear Cobalt
28 Complexes. *Angew. Chem. Int. Ed.*, 2013, **52**, 11290-11293.
29
30 <https://doi.org/10.1002/anie.201303005>.
31
32 62. A. T. Hand, Ph.D., Investigation of Molecular Transition Metal Complexes: Structures,
33 Magnetic Properties, and Reactivities. University of Tennessee, Knoxville, 2024.
34
35 https://trace.tennessee.edu/utk_graddiss/10463/.
36
37 63. N. Malinová, J. Juráková, B. Brachňáková, J. D. Midlíková, E. Čížmár, V. T. Santana, R.
38 Herchel, M. Orlita, I. Mohelský, J. Moncol, P. Neugebauer and I. Šalitroš, Magnetization
39 Slow Dynamics in Mononuclear Co(II) Field-Induced Single-Molecule Magnet. *Cryst.*
40 *Growth Des.*, 2023, **23**, 2430-2441. <https://doi.org/10.1021/acs.cgd.2c01388>.
41
42 64. C. Rajnák, J. Titiš, J. Miklovič, G. E. Kostakis, O. Fuhr, M. Ruben and R. Boča, Five
43 mononuclear pentacoordinate Co(II) complexes with field-induced slow magnetic
44 relaxation. *Polyhedron*, 2017, **126**, 174-183. <https://doi.org/10.1016/j.poly.2017.01.028>.
45
46 65. K. Choroba, J. Palion-Gazda, B. Machura, A. Bieńko, D. Wojtala, D. Bieńko, C. Rajnák,
47 R. Boča, A. Ozarowski and M. Ozerov, Large Magnetic Anisotropy in Mono- and
48 Binuclear cobalt(II) Complexes: The Role of the Distortion of the Coordination Sphere in
49
50
51
52
53
54
55
56
57
58
59
60

- Validity of the Spin-Hamiltonian Formalism. *Inorg. Chem.*, 2024, **63**, 1068-1082.
<https://doi.org/10.1021/acs.inorgchem.3c03405>.
66. A. Dey, J. Ali, S. Moorthy, J. F. Gonzalez, F. Pointillart, S. K. Singh and V. Chandrasekhar, Field induced single ion magnet behavior in Co^{II} complexes in a distorted square pyramidal geometry. *Dalton Trans.*, 2023, **52**, 14807-14821.
<http://doi.org/10.1039/D3DT01769A>.
67. A. Świtlicka, B. Machura, M. Penkala, A. Bieńko, D. C. Bieńko, J. Titiš, C. Rajnák, R. Boča, A. Ozarowski and M. Ozerov, Slow Magnetic Relaxation in Cobalt(II) Field-Induced Single-Ion Magnets with Positive Large Anisotropy. *Inorg. Chem.*, 2018, **57**, 12740-12755. <https://doi.org/10.1021/acs.inorgchem.8b01906>.
68. Y. Cui, Y. Xu, X. Liu, Y. Li, B.-L. Wang, Y. Dong, W. Li and S. Lei, Field-Induced Single-Ion Magnetic Behavior in Two Mononuclear Cobalt(II) Complexes. *Chem. Asian J.*, 2019, **14**, 2620-2628. <https://doi.org/10.1002/asia.201900258>.
69. P. Gast and E. J. J. Groenen, EPR Interactions – Anisotropy. *eMagRes*, 2016, **5**, 1435-1444. <https://doi.org/10.1002/9780470034590.emrstm1500>.
70. C. N. Widener, A. N. Bone, M. Ozerov, R. Richardson, Z. Lu, K. Thirunavukkuarasu, D. Smirnov, X.-T. Chen and Z.-L. Xue, Direct Observation of Magnetic Transitions in a Nickel(II) Complex with Large Anisotropy. *Chin. J. Inorg. Chem.*, 2020, **35**, 1149-1156.
<http://doi.org/10.11862/CJIC.2020.126>.
71. K. E. R. Marriott, L. Bhaskaran, C. Wilson, M. Medarde, S. T. Ochsenein, S. Hill and M. Murrie, Pushing the limits of magnetic anisotropy in trigonal bipyramidal Ni(II). *Chem. Sci.*, 2015, **6**, 6823-6828. <http://doi.org/10.1039/C5SC02854J>.
72. G. A. Craig, A. Sarkar, C. H. Woodall, M. A. Hay, K. E. R. Marriott, K. V. Kamenev, S. A. Moggach, E. K. Brechin, S. Parsons, G. Rajaraman and M. Murrie, Probing the origin of the giant magnetic anisotropy in trigonal bipyramidal Ni(II) under high pressure. *Chem. Sci.*, 2018, **9**, 1551-1559. <http://doi.org/10.1039/C7SC04460G>.
73. M. Georgiev and H. Chamati, Magnetic Behavior of Trigonal (Bi-)pyramidal 3d⁸ Mononuclear Nanomagnets: The Case of [Ni(MDABCO)₂Cl₃]ClO₄. *ACS Omega*, 2023, **8**, 28640-28650. <https://doi.org/10.1021/acsomega.3c03208>.
74. N. Lau, Y. Sano, J. W. Ziller and A. S. Borovik, Terminal Ni^{II}-OH/-OH₂ complexes in trigonal bipyramidal geometries derived from H₂O. *Polyhedron*, 2017, **125**, 179-185.
<https://doi.org/10.1016/j.poly.2016.11.015>.

- 1
2
3 75. S. Gómez-Coca, E. Cremades, N. Aliaga-Alcalde and E. Ruiz, Huge Magnetic
4 Anisotropy in a Trigonal-Pyramidal Nickel(II) Complex. *Inorg. Chem.*, 2014, **53**, 676-678.
5 <https://doi.org/10.1021/ic402256v>.
6
7
8 76. B. Cahier, M. Perfetti, G. Zakhia, D. Naoufal, F. El-Khatib, R. Guillot, E. Rivière, R.
9 Sessoli, A.-L. Barra, N. Guihéry and T. Mallah, Magnetic Anisotropy in Pentacoordinate
10 Ni^{II} and Co^{II} Complexes: Unraveling Electronic and Geometrical Contributions. *Chem.*
11 *Eur. J.*, 2017, **23**, 3648-3657. <https://doi.org/10.1002/chem.201604872>.
12
13
14 77. A. Escuer, R. Vicente, M. Salah El Fallah, X. Solans and M. Font-Bardia, Synthesis,
15 structure and magnetic properties of several nickel-azido complexes with tetraamines as
16 blocking ligands. *Inorg. Chim. Acta*, 1996, **247**, 85-91. [https://doi.org/10.1016/0020-](https://doi.org/10.1016/0020-1693(95)04945-2)
17 [1693\(95\)04945-2](https://doi.org/10.1016/0020-1693(95)04945-2).
18
19
20 78. D. C. Lacy, Y. J. Park, J. W. Ziller, J. Yano and A. S. Borovik, Assembly and Properties
21 of Heterobimetallic Co^{II/III}/Ca^{II} Complexes with Aquo and Hydroxo Ligands. *J. Am. Chem.*
22 *Soc.*, 2012, **134**, 17526-17535. <https://doi.org/10.1021/ja304525n>.
23
24
25 79. Y. J. Park, S. A. Cook, N. S. Sickerman, Y. Sano, J. W. Ziller and A. S. Borovik,
26 Heterobimetallic Complexes with M(III)-(μ-OH)-M(II) Cores (M(III) = Fe, Mn, Ga; M(II) =
27 Ca, Sr, and Ba): Structural, Kinetic, and Redox Properties. *Chem. Sci.*, 2013, **4**, 717-
28 726. <https://doi.org/10.1039/C2SC21400H>.
29
30
31 80. J. Krzystek and J. Telser, Measuring giant anisotropy in paramagnetic transition metal
32 complexes with relevance to single-ion magnetism. *Dalton Trans.*, 2016, **45**, 16751-
33 16763. <https://doi.org/10.1039/C6DT01754A>.
34
35
36 81. A. T. Hand, B. D. Watson-Sanders and Z.-L. Xue, Spectroscopic techniques to probe
37 magnetic anisotropy and spin-phonon coupling in metal complexes. *Dalton Trans.*,
38 2024, **53**, 4390-4405. <http://doi.org/10.1039/D3DT03609J>.
39
40
41 82. J. Krzystek, A. Ozarowski and J. Telser, Multi-frequency, high-field EPR as a powerful
42 tool to accurately determine zero-field splitting in high-spin transition metal coordination
43 complexes. *Coord. Chem. Rev.*, 2006, **250**, 2308-2324.
44 <https://doi.org/10.1016/j.ccr.2006.03.016>.
45
46
47 83. T. Dubroca, A. Ozarowski, Y. Sunatsuki, J. Telser, S. Hill and J. Krzystek, Benefitting
48 from Magnetic Field-Induced Torquing in Terahertz EPR of a Mn^{III} Coordination
49 Complex. *Appl. Magn. Reson.*, 2025, **56**, 137-149., [https://doi.org/10.1007/s00723-024-](https://doi.org/10.1007/s00723-024-01706-3)
50 [01706-3](https://doi.org/10.1007/s00723-024-01706-3).
51
52
53 84. A. N. Bone, C. N. Widener, D. H. Moseley, Z. Liu, Z. Lu, Y. Cheng, L. L. Daemen, M.
54 Ozerov, J. Telser, K. Thirunavukkuarasu, D. Smirnov, S. M. Greer, S. Hill, J. Krzystek, K.
55
56
57
58
59
60

- Holldack, A. Aliabadi, A. Schnegg, K. R. Dunbar and Z.-L. Xue, Applying Unconventional Spectroscopies to the Single-Molecule Magnets $\text{Co}(\text{PPh}_3)_2\text{X}_2$ (X = Cl, Br, I): Unveiling Magnetic Transitions and Spin-Phonon Coupling. *Chem. Eur. J.*, 2021, **27**, 11110-11125. <https://doi.org/10.1002/chem.202100705>.
85. W. Lv, L. Chen, X.-T. Chen, H. Yan, Z. Wang, Z.-W. Ouyang and Z.-L. Xue, Structures and magnetic anisotropies of two seven-coordinate $\text{Co}(\text{II})$ -nitrate complexes showing slow magnetic relaxation. *New J. Chem.*, 2023, **47**, 15553-15560. <http://doi.org/10.1039/D3NJ02160B>.
86. H.-H. Cui, Y.-Q. Zhang, X.-T. Chen, Z. Wang and Z.-L. Xue, Magnetic anisotropy and slow magnetic relaxation processes of cobalt(II)-pseudohalide complexes. *Dalton Trans.*, 2019, **48**, 10743-10752. <http://doi.org/10.1039/C9DT00644C>.
87. S.-Y. Chen, H.-H. Cui, Y.-Q. Zhang, Z. Wang, Z.-W. Ouyang, L. Chen, X.-T. Chen, H. Yan and Z.-L. Xue, Magnetic anisotropy and relaxation behavior of six-coordinate tris(pivalato)- $\text{Co}(\text{II})$ and - $\text{Ni}(\text{II})$ complexes. *Dalton Trans.*, 2018, **47**, 10162-10171. <http://doi.org/10.1039/C8DT01554F>.
88. Y. Rechkemmer, F. D. Breitgoff, M. van der Meer, M. Atanasov, M. Hakl, M. Orlita, P. Neugebauer, F. Neese, B. Sarkar and J. van Slageren, A Four-Coordinate Cobalt(II) Single-Ion Magnet with Coercivity and a Very High Energy Barrier. *Nat. Commun.*, 2016, **7**, 10467. <http://doi.org/10.1038/ncomms10467>.
89. P. C. Bunting, M. Atanasov, E. Damgaard-Møller, M. Perfetti, I. Crassee, M. Orlita, J. Overgaard, J. van Slageren, F. Neese and J. R. Long, A linear cobalt(II) complex with maximal orbital angular momentum from a non-Aufbau ground state. *Science*, 2018, **362**, eaat7319. <https://doi.org/10.1126/science.aat7319>.
90. S. E. Stavretis, D. H. Moseley, F. Fei, H.-H. Cui, Y. Cheng, A. A. Podlesnyak, X. Wang, L. L. Daemen, C. M. Hoffmann, M. Ozerov, Z. Lu, K. Thirunavukkuarasu, D. Smirnov, T. Chang, Y.-S. Chen, A. J. Ramirez-Cuesta, X.-T. Chen and Z.-L. Xue, Spectroscopic Studies of the Magnetic Excitation and Spin-Phonon Couplings in a Single-Molecule Magnet. *Chem. Eur. J.*, 2019, **25**, 15846-15857. <https://doi.org/10.1002/chem.201903635>.
91. A. N. Bone, S. E. Stavretis, J. Krzystek, Z. Liu, Q. Chen, Z. Gai, X. Wang, C. A. Steren, X. B. Powers, A. A. Podlesnyak, X.-T. Chen, J. Telsler, H. Zhou and Z.-L. Xue, Manganese tetraphenylporphyrin bromide and iodide. Studies of structures and magnetic properties. *Polyhedron*, 2020, **184**, 114488. <https://doi.org/10.1016/j.poly.2020.114488>.

- 1
2
3 92. P. Tin, S. E. Stavretis, M. Ozerov, J. Krzystek, A. N. Ponomaryov, S. A. Zvyagin, J.
4 Wosnitza, C.-C. Chen, P. P. Y. Chen, J. Telser and Z.-L. Xue, *Advanced Magnetic*
5 *Resonance Studies of Tetraphenylporphyrinatoiron(III) Halides. Appl. Magn. Reson.*,
6 2020, **51**, 1411-1432. <https://doi.org/10.1007/s00723-020-01236-8>.
7
8
9 93. M. Viciano-Chumillas, G. Blondin, M. Clémancey, J. Krzystek, M. Ozerov, D. Armentano,
10 A. Schnegg, T. Lohmiller, J. Telser, F. Lloret and J. Cano, *Single-Ion Magnetic*
11 *Behaviour in an Iron(III) Porphyrin Complex: A Dichotomy Between High Spin and 5/2–*
12 *3/2 Spin Admixture. Chem. Eur. J.*, 2020, **26**, 14242-14251.
13 <https://doi.org/10.1002/chem.202003052>.
14
15
16
17 94. K. D. Hughey, N. C. Harms, K. R. O'Neal, A. J. Clune, J. C. Monroe, A. L. Blockmon, C.
18 P. Landee, Z. Liu, M. Ozerov and J. L. Musfeldt, *Spin–Lattice Coupling Across the*
19 *Magnetic Quantum-Phase Transition in Copper-Containing Coordination Polymers.*
20 *Inorg. Chem.*, 2020, **59**, 2127-2135. <https://doi.org/10.1021/acs.inorgchem.9b02394>.
21
22
23 95. J. Vallejo, M. Viciano-Chumillas, F. Lloret, M. Julve, I. Castro, J. Krzystek, M. Ozerov, D.
24 Armentano, G. De Munno and J. Cano, *Coligand Effects on the Field-Induced Double*
25 *Slow Magnetic Relaxation in Six-Coordinate Cobalt(II) Single-Ion Magnets (SIMs) with*
26 *Positive Magnetic Anisotropy. Inorg. Chem.*, 2019, **58**, 15726-15740.
27 <https://doi.org/10.1021/acs.inorgchem.9b01719>.
28
29
30
31 96. L. Devkota, D. J. SantaLucia, A. M. Wheaton, A. J. Pienkos, S. V. Lindeman, J.
32 Krzystek, M. Ozerov, J. F. Berry, J. Telser and A. T. Fiedler, *Spectroscopic and*
33 *Magnetic Studies of Co(II) Scorpionate Complexes: Is There a Halide Effect on Magnetic*
34 *Anisotropy? Inorg. Chem.*, 2023, **62**, 5984-6002.
35 <https://doi.org/10.1021/acs.inorgchem.2c04468>.
36
37
38 97. E. Ferentinos, D. Tzeli, S. Sottini, E. J. J. Groenen, M. Ozerov, G. Poneti, K. Kaniewska-
39 Laskowska, J. Krzystek and P. Kyritsis, *Magnetic anisotropy and structural flexibility in*
40 *the field-induced single ion magnets [Co{(OPPh₂)(EPPH₂)N₂]₂], E = S, Se, explored by*
41 *experimental and computational methods. Dalton Trans.*, 2023, **52**, 2036-2050.
42 <http://doi.org/10.1039/D2DT03335F>.
43
44
45
46 98. A. Landart-Gereka, M. M. Quesada-Moreno, M. A. Palacios, I. F. Díaz-Ortega, H. Nojiri,
47 M. Ozerov, J. Krzystek and E. Colacio, *Pushing up the easy-axis magnetic anisotropy*
48 *and relaxation times in trigonal prismatic Co^{II} mononuclear SMMs by molecular structure*
49 *design. Chem. Commun.*, 2023, **59**, 952-955. <http://doi.org/10.1039/D2CC06012D>.
50
51
52
53
54
55
56
57
58
59
60

- 1
2
3
4
5
6
7
8
9
10
11
12
13
14
15
16
17
18
19
20
21
22
23
24
25
26
27
28
29
30
31
32
33
34
35
36
37
38
39
40
41
42
43
44
45
46
47
48
49
50
51
52
53
54
55
56
57
58
59
60
99. J. G. C. Kragoskow, J. Marbey, C. D. Buch, J. Nehrkorn, M. Ozerov, S. Piligkos, S. Hill and N. F. Chilton, Analysis of vibronic coupling in a 4f molecular magnet with FIRMS. *Nat. Commun.*, 2022, **13**, 825. <https://doi.org/10.1038/s41467-022-28352-2>.
100. M. Perfetti, M. Gysler, Y. Rechkemmer-Patalen, P. Zhang, H. Taştan, F. Fischer, J. Netz, W. Frey, L. W. Zimmermann, T. Schleid, M. Haki, M. Orlita, L. Ungur, L. Chibotaru, T. Brock-Nannestad, S. Piligkos and J. van Slageren, Determination of the electronic structure of a dinuclear dysprosium single molecule magnet without symmetry idealization. *Chem. Sci.*, 2019, **10**, 2101-2110. <http://doi.org/10.1039/C8SC03170C>.
101. P. Baltzer, A. Furrer, J. Hulliger and A. Stebler, Magnetic properties of nickelocene. A reinvestigation using inelastic neutron scattering and magnetic susceptibility. *Inorg. Chem.*, 1988, **27**, 1543-1548. <https://doi.org/10.1021/ic00282a007>.
102. H. Andres, R. Basler, H.-U. Güdel, G. Aromí, G. Christou, H. Büttner and B. Rufflé, Inelastic neutron scattering and magnetic susceptibilities of the single-molecule magnets $[\text{Mn}_4\text{O}_3\text{X}(\text{OAc})_3(\text{dbm})_3]$ (X = Br, Cl, OAc, and F): Variation of the anisotropy along the series. *J. Am. Chem. Soc.*, 2000, **122**, 12469-12477. <http://dx.doi.org/10.1021/ja0009424>.
103. Z.-L. Xue, A. J. Ramirez-Cuesta, C. M. Brown, S. Calder, H. Cao, B. C. Chakoumakos, L. L. Daemen, A. Huq, A. I. Kolesnikov, E. Mamontov, A. A. Podlesnyak and X. Wang, Neutron Instruments for Research in Coordination Chemistry. *Eur. J. Inorg. Chem.*, 2019, DOI: 10.1002/ejic.201801076, 1065-1089. <https://doi.org/10.1002/ejic.201801076>.
104. G. Amoretti, R. Caciuffo, S. Carretta, T. Guidi, N. Magnani and P. Santini, Inelastic neutron scattering investigations of molecular nanomagnets. *Inorg. Chim. Acta.*, 2008, **361**, 3771-3776. <https://doi.org/10.1016/j.ica.2008.03.047>.
105. P. C. H. Mitchell, S. F. Parker, A. J. Ramirez-Cuesta and J. Tomkinson, *Vibrational Spectroscopy with Neutrons: With Applications in Chemistry, Biology, Materials Science and Catalysis*, World Scientific Publishing Company, 2005. <https://www.worldscientific.com/worldscibooks/10.1142/5628>.
106. M. A. Dunstan, R. A. Mole and C. Boskovic, Inelastic Neutron Scattering of Lanthanoid Complexes and Single-Molecule Magnets. *Eur. J. Inorg. Chem.*, 2019, **2019**, 1090-1105. <https://doi.org/10.1002/ejic.201801306>.
107. E. J. L. McInnes, Spectroscopy of Single-Molecule Magnets. *Struct. Bond. (Single-Molecule Magnets and Related Phenomena)*, 2006, DOI: 10.1007/430_034, 69-102. https://doi.org/10.1007/430_034.

- 1
2
3 108. E. Colacio, J. Ruiz, E. Ruiz, E. Cremades, J. Krzystek, S. Carretta, J. Cano, T. Guidi, W.
4 Wernsdorfer and E. K. Brechin, Slow Magnetic Relaxation in a Co^{II}-Y^{III} Single-Ion
5 Magnet with Positive Axial Zero-Field Splitting. *Angew. Chem. In. Ed.*, 2013, **52**, 9130-
6 9134. <https://doi.org/10.1002/anie.201304386>.
7
8
9 109. K. S. Pedersen, L. Ungur, M. Sigrist, A. Sundt, M. Schau-Magnussen, V. Vieru, H.
10 Mutka, S. Rols, H. Weihe, O. Waldmann, L. F. Chibotaru, J. Bendix and J. Dreiser,
11 Modifying the Properties of 4f Single-Ion Magnets by Peripheral Ligand
12 Functionalisation. *Chem. Sci.*, 2014, **5**, 1650-1660. <http://doi.org/10.1039/C3SC53044B>.
13
14
15 110. X. Feng, J.-L. Liu, K. S. Pedersen, J. Nehr Korn, A. Schnegg, K. Holldack, J. Bendix, M.
16 Sigrist, H. Mutka, D. Samohvalov, D. Aguilà, M.-L. Tong, J. R. Long and R. Clérac,
17 Multifaceted magnetization dynamics in the mononuclear complex [Re^{IV}Cl₄(CN)₂]²⁻.
18 *Chem. Commun.*, 2016, **52**, 12905-12908. <http://doi.org/10.1039/C6CC05473K>.
19
20
21 111. M. A. Sørensen, U. B. Hansen, M. Perfetti, K. S. Pedersen, E. Bartolomé, G. G.
22 Simeoni, H. Mutka, S. Rols, M. Jeong, I. Zivkovic, M. Retuerto, A. Arauzo, J. Bartolomé,
23 S. Piligkos, H. Weihe, L. H. Doerrer, J. van Slageren, H. M. Rønnow, K. Lefmann and J.
24 Bendix, Chemical tunnel-splitting-engineering in a dysprosium-based molecular
25 nanomagnet. *Nat. Commun.*, 2018, **9**, 1292. [https://doi.org/10.1038/s41467-018-03706-](https://doi.org/10.1038/s41467-018-03706-x)
26 [x](https://doi.org/10.1038/s41467-018-03706-x).
27
28
29 112. M. Perfetti, M. A. Sørensen, U. B. Hansen, H. Bamberger, S. Lenz, P. P. Hallmen, T.
30 Fennell, G. G. Simeoni, A. Arauzo, J. Bartolomé, E. Bartolomé, K. Lefmann, H. Weihe, J.
31 van Slageren and J. Bendix, Magnetic Anisotropy Switch: Easy Axis to Easy Plane
32 Conversion and Vice Versa. *Adv. Funct. Mater.*, 2018, **28**, 1801846.
33 <https://doi.org/10.1002/adfm.201801846>.
34
35
36 113. M. Vongi, M. J. Giansiracusa, W. Van den Heuvel, R. W. Gable, B. Moubaraki, K. S.
37 Murray, D. Yu, R. A. Mole, A. Soncini and C. Boskovic, Magnetic Excitations in
38 Polyoxotungstate-Supported Lanthanoid Single-Molecule Magnets: An Inelastic Neutron
39 Scattering and ab Initio Study. *Inorg. Chem.*, 2017, **56**, 378-394.
40 <https://doi.org/10.1021/acs.inorgchem.6b02312>.
41
42
43 114. M. Vongi, M. J. Giansiracusa, R. W. Gable, W. Van den Heuvel, K. Latham, B.
44 Moubaraki, K. S. Murray, D. Yu, R. A. Mole, A. Soncini and C. Boskovic, Ab initio
45 calculations as a quantitative tool in the inelastic neutron scattering study of a single-
46 molecule magnet analogue. *Chem. Commun.*, 2016, **52**, 2091-2094.
47 <http://doi.org/10.1039/C5CC07541F>.
48
49
50
51
52
53
54
55
56
57
58
59
60

- 1
2
3 115. N. A. Bonde, J. B. Petersen, M. A. Sørensen, U. G. Nielsen, B. Fåk, S. Rols, J. Ollivier,
4 H. Weihe, J. Bendix and M. Perfetti, Importance of Axial Symmetry in Elucidating
5 Lanthanide–Transition Metal Interactions. *Inorg. Chem.*, 2020, **59**, 235-243.
6 <https://doi.org/10.1021/acs.inorgchem.9b02064>.
7
8
9 116. S. C. Hunter, A. A. Podlesnyak and Z.-L. Xue, Magnetic Excitations in Metalloporphyrins
10 by Inelastic Neutron Scattering: Determination of Zero-Field Splittings in Iron,
11 Manganese, and Chromium Complexes. *Inorg. Chem.*, 2014, **53**, 1955-1961.
12 <https://doi.org/10.1021/ic4028354>.
13
14
15 117. S. E. Stavretis, M. Atanasov, A. A. Podlesnyak, S. C. Hunter, F. Neese and Z.-L. Xue,
16 Magnetic Transitions in Iron Porphyrin Halides by Inelastic Neutron Scattering and Ab
17 Initio Studies of Zero-Field Splittings. *Inorg. Chem.*, 2015, **54**, 9790-9801.
18 <https://doi.org/10.1021/acs.inorgchem.5b01505>.
19
20
21 118. S.-Y. Chen, W. Lv, H.-H. Cui, L. Chen, Y.-Q. Zhang, X.-T. Chen, Z. Wang, Z.-W.
22 Ouyang, H. Yan and Z.-L. Xue, Magnetic anisotropies and slow magnetic relaxation of
23 three tetrahedral tetrakis(pseudohalido)–cobalt(II) complexes. *New J. Chem.*, 2021, **45**,
24 16852-16861. <http://doi.org/10.1039/D1NJ01916C>.
25
26
27 119. R. Caciuffo, T. Guidi, G. Amoretti, S. Carretta, E. Livioti, P. Santini, C. Mondelli, G.
28 Timco, C. A. Muryn and R. E. P. Winpenny, Spin dynamics of heterometallic Cr 7 M
29 wheels (M= Mn, Zn, Ni) probed by inelastic neutron scattering. *Phys. Rev. B*, 2005, **71**,
30 174407. <https://doi.org/10.1103/PhysRevB.71.174407>.
31
32
33 120. W. R. Hagen, High-frequency EPR of transition ion complexes and metalloproteins.
34 *Coord. Chem. Rev.*, 1999, **190**, 209-229. [https://doi.org/10.1016/S0010-8545\(99\)00079-](https://doi.org/10.1016/S0010-8545(99)00079-X)
35 [X](https://doi.org/10.1016/S0010-8545(99)00079-X).
36
37
38 121. M. A. Spackman and D. Jayatilaka, Hirshfeld surface analysis. *CrystEngComm*, 2009,
39 **11**, 19-32. <https://doi.org/10.1039/B818330A>.
40
41
42 122. D. H. Moseley, S. E. Stavretis, Z. Zhu, M. Guo, C. M. Brown, M. Ozerov, Y. Cheng, L. L.
43 Daemen, R. Richardson and G. Knight, Inter-Kramers transitions and spin–phonon
44 couplings in a lanthanide-based single-molecule magnet. *Inorg. Chem.*, 2020, **59**, 5218-
45 5230. <https://doi.org/10.1021/acs.inorgchem.0c00523>.
46
47
48 123. S. E. Stavretis, D. H. Moseley, F. Fei, H. H. Cui, Y. Cheng, A. A. Podlesnyak, X. Wang,
49 L. L. Daemen, C. M. Hoffmann and M. Ozerov, Spectroscopic Studies of the Magnetic
50 Excitation and Spin-Phonon Couplings in a Single-Molecule Magnet. *Chem. Eur. J.*,
51 2019, **25**, 15846-15857. <https://doi.org/10.1002/chem.201903635>.
52
53
54
55
56
57
58
59
60

- 1
2
3 124. D. H. Moseley, S. E. Stavretis, K. Thirunavukkuarasu, M. Ozerov, Y. Cheng, L. L.
4 Daemen, J. Ludwig, Z. Lu, D. Smirnov, C. M. Brown, A. Pandey, A. J. Ramirez-Cuesta,
5 A. C. Lamb, M. Atanasov, E. Bill, F. Neese and Z.-L. Xue, Spin–phonon couplings in
6 transition metal complexes with slow magnetic relaxation. *Nat. Comm.*, 2018, **9**, 2572.
7 <https://doi.org/10.1038/s41467-018-04896-0>.
8
9
10
11 125. P. R. Spackman, M. J. Turner, J. J. McKinnon, S. K. Wolff, D. J. Grimwood, D.
12 Jayatilaka and M. A. Spackman, CrystalExplorer: a program for Hirshfeld surface
13 analysis, visualization and quantitative analysis of molecular crystals. *J. Appl.*
14 *Crystallogr.*, 2021, **54**, 1006-1011. <https://doi.org/10.1107/S1600576721002910>.
15
16
17 126. M. Darii, J. van Leusen, V. C. Kravtsov, Y. Chumakov, K. Krämer, S. Decurtins, S.-X.
18 Liu, P. Kögerler and S. G. Baca, {Mn^{III}Mn^{IV}Dy₂^{III}} Single-Molecule Magnet Based on
19 Cubane Subunits. *Cryst. Growth Des.*, 2023, **23**, 6944-6952.
20 <https://doi.org/10.1021/acs.cgd.3c00783>.
21
22
23 127. S. C. Hunter, B. A. Smith, C. M. Hoffmann, X. Wang, Y.-S. Chen, G. J. McIntyre and Z.-
24 L. Xue, Intermolecular Interactions in Solid-State Metalloporphyrins and Their Impacts
25 on Crystal and Molecular Structures. *Inorg. Chem.*, 2014, **53**, 11552-11562.
26 <https://doi.org/10.1021/ic5015835>.
27
28
29 128. C. T. Kelly, R. Jordan, S. Felton, H. Müller-Bunz and G. G. Morgan, Spontaneous Chiral
30 Resolution of a Mn^{III} Spin-Crossover Complex with High Temperature 80 K Hysteresis.
31 *Chem. Eur. J.*, 2023, **29**, e202300275. <https://doi.org/10.1002/chem.202300275>.
32
33
34 129. S. Ou, C. Wu, Z. Fan, J. Chen, H. Tian and X. Bao, Cooperative Spin Crossover Near
35 Room Temperature in Fe(II) Complexes Based on Acylhydrazone Ligands. *Cryst.*
36 *Growth Des.*, 2023, **23**, 3275-3283. <https://doi.org/10.1021/acs.cgd.2c01443>.
37
38
39 130. S. Roy, J. Du, E. M. Manohar, T. Aziz, T. K. Pal, L. Sun, N. Ahmed and S. Das,
40 Syntheses, Structures, and Magnetic Properties of Novel [3×1 + 2×1] Pentanuclear
41 Zinc(II)-Lanthanide(III) Cocrystal Complexes: Slow Magnetic Relaxation Behavior of the
42 Dy(III) Analogue. *Cryst. Growth Des.*, 2023, **23**, 2218-2230.
43 <https://doi.org/10.1021/acs.cgd.2c01256>.
44
45
46 131. H. Hagiwara, T. Matsuyama and T. Udagawa, Solvent Coligand-Induced Spin State
47 Variation in Iron(II) Complexes Bearing Pentadentate N5 Ligand Toward the
48 Construction of an N5O Spin Crossover Center. *Cryst. Growth Des.*, 2023, **23**, 1622-
49 1632. <https://doi.org/10.1021/acs.cgd.2c01239>.
50
51
52
53
54
55
56
57
58
59
60

- 1
2
3
4
5
6
7
8
9
10
11
12
13
14
15
16
17
18
19
20
21
22
23
24
25
26
27
28
29
30
31
32
33
34
35
36
37
38
39
40
41
42
43
44
45
46
47
48
49
50
51
52
53
54
55
56
57
58
59
60
132. J. Wang, Y. Li, R.-J. Wei, Z. Tang, Z.-S. Yao and J. Tao, Spin-Crossover Behaviors of Iron(II) Complexes Bearing Halogen Ligands in Solid State and Solution. *Inorg. Chem.*, 2023, **62**, 1354-1361. <https://doi.org/10.1021/acs.inorgchem.2c02815>.
133. D. Stati, J. van Leusen, N. Ahmed, V. C. Kravtsov, P. Kögerler and S. G. Baca, A {Co^{III}2Dy^{III}4} Single-Molecule Magnet with an Expanded Core Structure. *Cryst. Growth Des.*, 2023, **23**, 395-402. <https://doi.org/10.1021/acs.cgd.2c01085>.
134. S. Ghosh, S. Ghosh, S. Kamilya, S. Mandal, S. Mehta and A. Mondal, Impact of Counteranion on Reversible Spin-State Switching in a Series of Cobalt(II) Complexes Containing a Redox-Active Ethylenedioxythiophene-Based Terpyridine Ligand. *Inorg. Chem.*, 2022, **61**, 17080-17088. <https://doi.org/10.1021/acs.inorgchem.2c02313>.
135. F. Garci, H. Chebbi, N. Rouzbeh, L. Rochels, S. Disch, A. Klein and M. F. Zid, Structure, optical and magnetic properties of the pyridinium cobaltate (C₆H₉N₂)₂[CoCl₄]. *Inorg. Chim. Acta*, 2022, **539**, 121003. <https://doi.org/10.1016/j.ica.2022.121003>.
136. L. Spillecke, S. Tripathi, C. Koo, A. Bahr, A. Swain, R. Haldar, M. Ansari, J. Jasinski, G. Rajaraman, M. Shanmugam and R. Klingeler, Role of Coordination Geometry on the Magnetic Relaxation Dynamics of Isomeric Five-Coordinate Low-Spin Co(II) Complexes. *Inorg. Chem.*, 2022, **61**, 317-327. <https://doi.org/10.1021/acs.inorgchem.1c02881>.
137. S. Athira, D. J. Mondal, S. Shome, B. Dey and S. Konar, Effect of intermolecular anionic interactions on spin crossover of two triple-stranded dinuclear Fe(II) complexes showing above room temperature spin transition. *Dalton Trans.*, 2022, **51**, 16706-16713. <http://doi.org/10.1039/D2DT02115C>.
138. S. Ghosh, S. Bagchi, S. Kamilya, S. Mehta, D. Sarkar, R. Herchel and A. Mondal, Impact of counter anions on spin-state switching of manganese(III) complexes containing an azobenzene ligand. *Dalton Trans.*, 2022, **51**, 7681-7694. <http://doi.org/10.1039/D2DT00660J>.
139. N. Mavragani, D. Errulat, D. A. Gálico, A. A. Kitos, A. Mansikkamäki and M. Murugesu, Radical-Bridged Ln₄ Metallocene Complexes with Strong Magnetic Coupling and a Large Coercive Field. *Angew. Chem. Int. Ed.*, 2021, **60**, 24206-24213. <https://doi.org/10.1002/anie.202110813>.
140. O. V. Nesterova, O. Y. Vassilyeva, B. W. Skelton, A. Bieńko, A. J. L. Pombeiro and D. S. Nesterov, A novel o-vanillin Fe(III) complex catalytically active in C–H oxidation: exploring the magnetic exchange interactions and spectroscopic properties with different DFT functionals. *Dalton Trans.*, 2021, **50**, 14782-14796. <http://doi.org/10.1039/D1DT02366G>.

- 1
2
3 141. Z.-M. Yu, S.-Z. Zhao, Y.-T. Wang, P.-Y. Xu, C.-Y. Qin, Y.-H. Li, X.-H. Zhou and S.
4 Wang, Anion-driven supramolecular modulation of spin-crossover properties in
5 mononuclear iron(III) Schiff-base complexes. *Dalton Trans.*, 2021, **50**, 15210-15223.
6 <http://doi.org/10.1039/D1DT02394B>.
7
8 142. C. Rajnák, J. Titiš, J. Moncol', D. Valigura and R. Boča, Effect of the Distant Substituent
9 to Slow Magnetic Relaxation of Pentacoordinate Fe(III) Complexes. *Inorg. Chem.*, 2020,
10 **59**, 14871-14878. <https://doi.org/10.1021/acs.inorgchem.0c00647>.
11
12 143. R. Díaz-Torres, W. Phonsri, K. S. Murray, L. Liu, M. Ahmed, S. M. Neville, P. Harding
13 and D. J. Harding, Spin Crossover in Iron(III) Quinolyisalicylaldiminates: The Curious
14 Case of [Fe(qsal-F)₂](Anion). *Inorg. Chem.*, 2020, **59**, 13784-13791.
15 <https://doi.org/10.1021/acs.inorgchem.0c02201>.
16
17 144. J. D. Schneider, B. A. Smith, G. A. Williams, D. R. Powell, F. Perez, G. T. Rowe and L.
18 Yang, Synthesis and Characterization of Cu(II) and Mixed-Valence Cu(I)Cu(II) Clusters
19 Supported by Pyridylamide Ligands. *Inorg. Chem.*, 2020, **59**, 5433-5446.
20 <https://doi.org/10.1021/acs.inorgchem.0c00008>.
21
22 145. A. Banerjee, S. Banerjee, C. J. Gómez García, S. Benmansour and S. Chattopadhyay,
23 Field-induced single molecule magnet behavior of a dinuclear cobalt(II) complex: a
24 combined experimental and theoretical study. *Dalton Trans.*, 2020, **49**, 16778-16790.
25 <http://doi.org/10.1039/D0DT02158J>.
26
27 146. M. I. M. Shahid, M. Ahmad, Rahisuddin, R. Arif, S. Tasneem, F. Sama and I. A. Ansari,
28 Synthesis, crystal structures, photoluminescence, magnetic and antioxidant properties,
29 and theoretical analysis of Zn(II) and Cu(II) complexes of an aminoalcohol ligand
30 supported by benzoate counter anions. *New J. Chem.*, 2019, **43**, 622-633.
31 <http://doi.org/10.1039/C8NJ04122A>.
32
33 147. B. S. Sran, J. F. Gonzalez, V. Montigaud, B. Le Guennic, F. Pointillart, O. Cador and G.
34 Hundal, Structural and magnetic investigations of a binuclear coordination compound of
35 dysprosium(III) dinitrobenzoate. *Dalton Trans.*, 2019, **48**, 3922-3929.
36 <http://doi.org/10.1039/C8DT04253E>.
37
38 148. D. Maniaki, I. Mylonas-Margaritis, J. Mayans, A. Savvidou, C. P. Raptopoulou, V.
39 Bekiari, V. Psycharis, A. Escuer and S. P. Perlepes, Slow magnetic relaxation and
40 luminescence properties in lanthanide(III)/anil complexes. *Dalton Trans.*, 2018, **47**,
41 11859-11872. <http://doi.org/10.1039/C8DT01264D>.
42
43 149. G. C. Brackett, Ph.D., Far-Infrared Magnetic Resonance in Fe(III) and Mn(III)
44 Porphyrins, Myoglobin, Hemoglobin, Ferrichrome A, and Fe(III) Dithiocarbamates.
45
46
47
48
49
50
51
52
53
54
55
56
57
58
59
60

- Dissertation, University of California, Berkeley, 1970.
<https://escholarship.org/uc/item/2wt5m8qp>.
150. G. C. Brackett, P. L. Richards and W. S. Caughey, Far-Infrared Magnetic Resonance in Fe(III) and Mn(III) Porphyrins, Myoglobin, Hemoglobin, Ferrichrome A, and Fe(III) Dithiocarbamates. *J. Chem. Phys.*, 1971, **54**, 4383-4401.
<https://doi.org/10.1063/1.1674688>.
151. S. E. Stavretis, E. Mamontov, D. H. Moseley, Y. Cheng, L. L. Daemen, A. J. Ramirez-Cuesta and Z.-L. Xue, Effect of magnetic fields on the methyl rotation in a paramagnetic cobalt(II) complex. Quasielastic neutron scattering studies. *Phys. Chem. Chem. Phys.*, 2018, **20**, 21119-21126. <http://dx.doi.org/10.1039/C8CP01660G>.
152. P.-G. Reinhard and E. Suraud, *Gross Properties and Trends*, in *Introduction to Cluster Dynamics*, Wiley-VCH Verlag GmbH, 2008, pp. 133-178.
<http://dx.doi.org/10.1002/9783527602520.ch4>.
153. S. E. Stavretis, E. Mamontov, D. H. Moseley, Y. Cheng, L. L. Daemen, A. J. Ramirez-Cuesta and Z.-L. Xue, Effect of magnetic fields on the methyl rotation in a paramagnetic cobalt(II) complex. Quasielastic neutron scattering studies. *Phys. Chem. Chem. Phys.*, 2018, **20**, 21119-21126. <http://doi.org/10.1039/C8CP01660G>.
154. M. R. Saber and K. R. Dunbar, Ligands effects on the magnetic anisotropy of tetrahedral cobalt complexes. *Chem. Commun.*, 2014, **50**, 12266-12269.
<http://doi.org/10.1039/C4CC05724D>.
155. L. Chen, J. Wang, J.-M. Wei, W. Wernsdorfer, X.-T. Chen, Y.-Q. Zhang, Y. Song and Z.-L. Xue, Slow Magnetic Relaxation in a Mononuclear Eight-Coordinate Cobalt(II) Complex. *J. Am. Chem. Soc.*, 2014, **136**, 12213-12216.
<https://doi.org/10.1021/ja5051605>.
156. Y. J. Park, J. W. Ziller and A. S. Borovik, The Effects of Redox-Inactive Metal Ions on the Activation of Dioxygen: Isolation and Characterization of a Heterobimetallic Complex Containing a MnIII-(μ -OH)-CaII Core. *J. Am. Chem. Soc.*, 2011, **133**, 9258-9261.
<https://doi.org/10.1021/ja203458d>.
157. A. K. Hassan, L. A. Pardi, J. Krzystek, A. Sienkiewicz, P. Goy, M. Rohrer and L. C. Brunel, Ultrawide Band Multifrequency High-Field EMR Technique: A Methodology for Increasing Spectroscopic Information. *J. Magn. Reson.*, 2000, **142**, 300-312.
<https://doi.org/10.1006/jmre.1999.1952>.

- 1
2
3 158. G. Kresse and J. Furthmüller, Efficient iterative schemes for ab initio total-energy
4 calculations using a plane-wave basis set. *Phys. Rev. B*, 1996, **54**, 11169-11186.
5 <https://doi.org/10.1103/PhysRevB.54.11169>.
6
7
8 159. P. E. Blöchl, Projector augmented-wave method. *Phys. Rev. B*, 1994, **50**, 17953-17979.
9 <https://doi.org/10.1103/PhysRevB.50.17953>.
10
11 160. G. Kresse and D. Joubert, From ultrasoft pseudopotentials to the projector augmented-
12 wave method. *Phys. Rev. B*, 1999, **59**, 1758-1775.
13 <https://doi.org/10.1103/PhysRevB.59.1758>.
14
15
16 161. J. P. Perdew, K. Burke and M. Ernzerhof, Generalized Gradient Approximation Made
17 Simple. *Phys. Rev. Lett.*, 1996, **77**, 3865-3868.
18 <https://doi.org/10.1103/PhysRevLett.77.3865>.
19
20
21 162. J. Klimeš, D. R. Bowler and A. Michaelides, Chemical accuracy for the van der Waals
22 density functional. *J. Phys. Cond. Matt.*, 2010, **22**, 022201. [https://doi.org/10.1088/0953-](https://doi.org/10.1088/0953-8984/22/2/022201)
23 [8984/22/2/022201](https://doi.org/10.1088/0953-8984/22/2/022201).
24
25
26 163. A. Togo and I. Tanaka, First principles phonon calculations in materials science. *Scr.*
27 *Mater.*, 2015, **108**, 1-5. <https://doi.org/10.1016/j.scriptamat.2015.07.021>.
28
29
30 164. Y. Q. Cheng, L. L. Daemen, A. I. Kolesnikov and A. J. Ramirez-Cuesta, Simulation of
31 Inelastic Neutron Scattering Spectra Using OCLIMAX. *J. Chem. Theory Comput.*, 2019,
32 **15**, 1974-1982. <https://doi.org/10.1021/acs.jctc.8b01250>.
33
34
35
36
37
38
39
40
41
42
43
44
45
46
47
48
49
50
51
52
53
54
55
56
57
58
59
60

Data availability statement

Data are available from the authors upon request. The authors confirm that the data supporting the findings of this study are available within the article and its electronic supplementary materials (ESI).

1
2
3
4
5
6
7
8
9
10
11
12
13
14
15
16
17
18
19
20
21
22
23
24
25
26
27
28
29
30
31
32
33
34
35
36
37
38
39
40
41
42
43
44
45
46
47
48
49
50
51
52
53
54
55
56
57
58
59
60